



## Hidden archives in the cave: sediments, bat guano, and prehistoric footprints at the *ponte di Veja* complex (Verona, Italy)

Dario Battistel <sup>a,\*</sup> , Mara Bortolini <sup>b</sup> , Anna De Rossi <sup>b</sup>, Michele Bassetti <sup>c</sup>, Pietro Riello <sup>d</sup>, Marta Radaelli <sup>a</sup>, Andrea Pereswiet-Soltan <sup>e</sup> , Leonardo Latella <sup>f</sup>, Mauro Buonincontri <sup>g</sup> , Francesco Sauro <sup>b</sup> , Paola Salzani <sup>h</sup>, Elisabetta Cilli <sup>i</sup>, Marco Peresani <sup>j,k</sup> , Elena Ghezzo <sup>b</sup>

<sup>a</sup> Department of Environmental Sciences, Informatics and Statistics, Ca' Foscari University of Venice, Via Torino, 155 Mestre, Venice, 30172, Italy

<sup>b</sup> Department of Geosciences, University of Padova, Via Gradenigo 6, 35131, Padova, Italy

<sup>c</sup> CORA Società Archeologica S.r.l., Via Salisburgo 16, I-38121, Trento, Italy

<sup>d</sup> Department of Molecular Sciences and Nanosystems Ca' Foscari University of Venice, Via Torino 155, Mestre, Venezia, 30172, Italy

<sup>e</sup> Institute of Systematics and Evolution of Animals, Polish Academy of Sciences, Stakowska 17, 31-016, Krakow, Poland

<sup>f</sup> Museo di Storia Naturale di Verona, Department of Zoology, Lungadige Porta Vittoria 9, 37129, Verona, Italy

<sup>g</sup> Department of History and Cultural Heritage, University of Siena, Via Roma 47, Siena, 53100, Italy

<sup>h</sup> Soprintendenza Archeologia, Belle Arti e Paesaggio di Verona, Rovigo e Vicenza, Italy

<sup>i</sup> Department of Cultural Heritage, University of Bologna, Via Degli Ariani 1, 48121, Ravenna (RA), Italy

<sup>j</sup> Prehistoric and Anthropological Science Unit, Department of Humanities, University of Ferrara, Corso Ercole I D'Este, 32, I-44121, Ferrara, Italy

<sup>k</sup> Institute of Environmental Geology and Geoengineering, National Research Council, Piazza Della Scienza 1, 20126, Milano, Italy

### ARTICLE INFO

Handling Editor: Dr Donatella Magri

#### Keywords:

Ponte di veja

Cave sediment

Geochemical stratigraphy

Upper pleistocene

Epigravettian

### ABSTRACT

Cave A at Ponte di Veja (Verona, Italy) preserves a stratified record that links sediment dynamics, chemical alteration and Late-Pleistocene hunter-gatherer activity on the southern Alpine foreland. Integrated sedimentological, micromorphological, mineralogical and geochemical analyses show that the lowermost unit is an allochthonous loess- and soil-derived deposit emplaced at the Last Glacial Maximum by slow percolation from the karst plateau and later modified under hydromorphic conditions. It is overlain by a paleosol, whose abundant charcoal, organic matter and faunal signals indicate repeated human and large-mammal presence in addition to bat guano input. Uneven guano accumulation drives strong in-situ acidification, leaching of alkaline-earth elements and precipitation of taranakite in the wetter, more acidic cave sector, while carbonate buffering keeps isolated spots near neutral. The data support a four-stage depositional model. Quiet loess infill before the Bølling–Allerød interstadial, post-glacial runoff erosion, re-occupation by humans and bats during the Bølling–Allerød and Holocene, and mid-20th-century removal of much guano-charcoal sediment for fertiliser. Radiocarbon and anthracological evidence reveal Epigravettian exploitation that intensified with interstadial warming, contracted, but likely did not cease, during the Younger Dryas, and resumed under Holocene thermophilous woodland.

### 1. Introduction

Cave environments are complex systems influenced both by natural and anthropogenic factors (Torok et al., 2024; Biagioli et al., 2023; Moldovan et al., 2018). All caves differ from each other and oftentimes each cave is considered as a unique system. Cave mineral deposits (*i.e.* clastic or chemical, as defined by White, 2007), found in sediments or speleothems, have been recognized for their capacity to gather and preserve paleoenvironmental and paleoclimate information (Baker

et al., 2021; Duan et al., 2013), acting as natural traps for external materials. In particular, sediment deposition in cave can arise from various factors, including rock fall and frost shattering fluvial processes from rainfall, water percolation, and/or aeolian transport. In addition to mineral components, organic substances from microorganisms (*e.g.*, fungi), bat guano, insects and botanical remains (*e.g.*, pollen, wood, leaves), as well as other faunal residues such as bones contribute to the formation of the deposit (Farrand, 2001; White, 2007; Ghezzo et al., 2014; Moldovan et al., 2011; Bella et al., 2021).

\* Corresponding author.

E-mail address: [dario.battistel@unive.it](mailto:dario.battistel@unive.it) (D. Battistel).

Moreover, when caves are sporadically or habitually occupied by humans over centuries or millennia, anthropogenic residues such as pottery, stone tools, and charcoal fragments, brought intentionally or produced within the cave, become part of the deposit (Medina-Alcaide et al., 2023; Deldicque et al., 2022). Therefore, the analysis of sediment sequences and stratigraphy found in caves has a significant role in paleontological, geological, and archaeological research (Riordan et al., 2021; Stephens et al., 2017). A significant example of these principles is provided by the Veja karstic system (*Ponte di Veja*), north of Verona, Italy, whose multi-cave complex preserves a rich stratigraphic archive.

Since the first half of the 20th century, the *Ponte di Veja* complex has been recognized as a significant archaeological site for investigating prehistoric human activity in Lessinia. Stone tools and faunal remains found in the area suggest that Neanderthal and Sapiens hunter-gatherers groups settled the Lessinia since the Middle Pleistocene (Margaritora et al., 2020 and references therein; Falgueres et al., 2025). In Veja Cave A and in the surroundings of *Ponte di Veja*, Middle and Upper Palaeolithic chert tools were described by Bartolomei and Broglio (Broglio et al., 1963; Bartolomei and Broglio, 1975). In Valpantena Valley, Riparo Tagliente contains a long stratigraphic cultural sequence spanning from the Mousterian to the late Epigravettian (Fontana et al., 2018a). Further inside the valley bottom, the settlement of *Lugo di Grezzana* revealed human presence during the Neolithic (~5000 BC) (Pedrotti et al., 2015). The Bronze age in the *Ponte di Veja* and the surroundings is documented by tools and pottery fragments dating back to the 2nd-3rd millennium BC (Salzani, 1987). Specifically in Veja Cave A, although archaeological evidence relates to Neanderthals, no further information is currently

available about the chronology and the purposes of these frequentations. Upper Palaeolithic hunter-gatherers left dispersed traces as well, ascribable to the Epigravettian (Bartolomei and Broglio, 1975).

Stone tools found in the area suggest that Neanderthal hunters were present before 40,000 years ago (Romandini et al., 2012; Chelidonio, 1992), with the oldest evidence of stone tools dating to 54,000 years ago (Peresani et al., 2009). The abundance of fossil remains, including cave bear (*Ursus spelaeus*) (Galli et al., 2005) and wolves, provides insights into human-fauna coexistence during the glacial period, as investigated in the framework of the REFINd project (<https://pric.unive.it/project/s/refind/home>).

Despite the site's relevance to multiple disciplines, such as palaeontology, ecology and archaeology, detailed investigations of the sedimentary deposits in the *Ponte di Veja* complex, particularly in Cave A, remain scarce (see for example Cavallo et al., 2021 and references therein). The aim of this paper is twofold: (i) to characterize the sedimentary deposits in Cave A to determine the source of the sediment, the in-situ chemical alteration, and the dynamics of deposition (ii) drawing on the deposition processes, as well as on charcoal  $^{14}\text{C}$  dates and anthracological data, to investigate the prehistoric faunal and human occupation in relation to the environmental variability. Our research involves stratigraphic and micromorphological analyses, examination of the mineralogical and chemical composition of both sediments and guano, as well as the study of charcoal fragments.



## Cave A

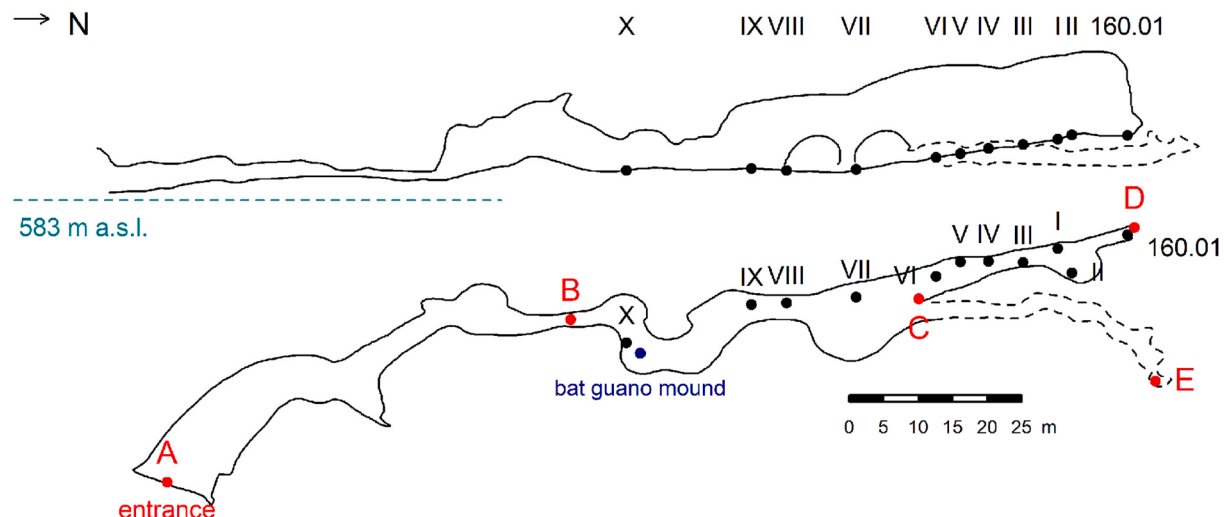


**Fig. 1.** Top: location and picture of the *Ponte di Veja* (VR, Italy). Bottom: map (section and base of the Cave A, including the position of the sampling sites). Roman numerals (I-X) refer to the location of the sampling site, while 160.01 refers to the trench excavated in 2022. Alphabetic labels (A-E) are used to identify section references within the cave, which are discussed in the following sections.

## 2. Methodology

### 2.1. Study site

Veja is a karstic system located north of Verona (Italy) (Fig. 1) at about 585 m above sea level (45.6081, 10.9702, EPSG: 3857). It consists of a series of at least five caves primarily oriented from north to south. A narrow valley interrupts the cave system, opening eastward into the *Marciora* valley and spanned by the Veja Bridge (*Ponte di Veja*), a geological formation remaining from the collapsed vault of a cave chamber. Grotta A (Cave cadastral number: 117 V/VR), also known as Veja Cave (*Grotta di Veja*) or Cave of the Bear (*Grotta dell'Orso*), is the main tunnel in the system, starting just below the north side of the bridge and extending approximately 180 m northward (Fabbri et al., 2017). This cavity formed through karst processes in the carbonate San Vigilio Oolite lithotype, with the vault and walls likely shaped by condensation-corrosion processes. An Eocene basaltic dike along the left wall influenced corrosion processes for nearly half the length of the cave. Within the Veja Cave, a shorter corridor branches off about halfway along the main tunnel to the east, with a slight water flow eroding soil deposits towards the cave entrance. As a result, Quaternary sediments are partly removed and reworked from this point towards the exit, leaving primary strata preserved only in the innermost cave areas (Ghezzo et al. in preparation).

A recent survey inside Cave A confirmed traces of an unauthorized excavation in the innermost section of the main tunnel, with reworked sediments and several bone fragments left on the surface. In 2022, E.G. of the Ca' Foscari University of Venice led a new excavation campaign of this area, designated trench 160.01, with the aim of cleaning the context and preparing the site for further research. The team divided the surface into quadrants, focusing on those interested by previous excavations, to rectify the reworked layers and document the stratigraphy. Subsequently, the removed sediment has been washed and screened, using sieves smaller than 1 mm, recovering bone fragments, teeth, charcoals, ochre, and lithic stones. The cave has also been studied for its zoological significance, particularly a bat colony (*Myotis myotis*, *Myotis blythii* and *Miniopterus schreibersii*), which occupies the cave from March to September, influencing the ecosystem through guano production that supports beetle and fly populations (Bertini et al., 2016).

### 2.2. Sample collection

During the fieldwork conducted in 2022, a trench approximately 1.10 m deep, hereinafter labelled 160.01, was excavated in the innermost portion of Cave A (see Fig. 1). After cleaning the sequence, we identified four distinct stratigraphic units (from SU-1 to SU-4, see afterwards). From trench 160.01, we collected a total of 16 sediment samples (~2 cm thick) of approximately 10 g each, covering SU-2A, SU-2B and part of SU-3. These samples were labelled 160.01.x, where x corresponds to the average depth in cm. All samples were freeze-dried, and visible charcoal fragments (approximately 0.5–8 mm) were picked and separated from the sediment. Accordingly, charcoal fragments collected from trench 160.01 were labelled as C-160.01.x. Physical (i.e. XRD) and chemical analyses (excluding pH and TOC% measurements) were carried out combining sediment samples 160.01.x from the same stratigraphic unit. Aiming to compare average geochemical signatures between stratigraphic units, where the number of subsamples per unit was uneven (e.g., SU-2B, n = 11; SU-3, n = 3), we pooled and homogenized subsamples within each unit to obtain a single representative composite. This approach is supported by preliminary TOC and pH analysis, where low intra unit variability was observed. Moreover, in the proximity of trench 160.01, a negative cylindrical interface with a width of 8 cm was found, tentatively interpreted as a posthole imprint. A large (~8 cm) charcoal fragment (C-PH), likely deriving from a structural vertical wooden element, anthropogenic in origin, was found in this posthole.

Based on the preliminary results obtained from trench 160.01, additional fieldwork was conducted in 2024, aiming to collect sediment samples along a ~75 m transect, excavating to a depth of 20–30 cm at ten spots as indicated in Fig. 1(I–X). The east-side lateral branch (section C-E in Fig. 1) was not considered in this study due to intense and more recent reworking of the deposit. Along the transect, an organic top layer, enriched in charcoal, similar to SU-2, was found at a depth ranging from 1 to ~10 cm. About 10 g of sediment from each spot, with a thickness of ~2 cm, was collected and hereinafter labelled as OS-i, where i corresponds to the sampling site (i.e. I–X). Only at spots I–IV, below the OS layer, a weakly clayey loam sediment with a texture similar to SU-3 was found. These samples are hereinafter labelled as SS-i, following the labelling scheme used for the OS samples. Although spots V–X were excavated to a depth of 20–30 cm, we were not able to identify the loamy sediment deposit, but encountered a mixture of complex, poorly defined structures, containing altered clay. In spots V–X, we only collected sediments from the OS layers. Additionally, we collected samples of ochre by scratching the vein that is visible in the wall of the cave, in proximity of spot I as well as a sample (~1g) from the carbonate cave ceiling. After freeze-drying and removing visible charcoal fragments (accordingly labelled as C-OS-i and C-SS-i), the sediments were ground, sieved at 2 mm, homogenized, and stored at 4 °C before physical and chemical analysis. Larger charcoal fragments were cut in half; one half was used for radiocarbon dating, while the other half was archived for further analysis.

Near spot XI, a bat guano mound about 1.5 m high and 3 m wide was found. The guano deposit was horizontally cored with a 40 mm diameter plastic tube until the centre of the mound was reached at a height of about 80 cm from the bottom. The guano samples were freeze-dried and homogenized; three aliquots were used for chemical analysis. A ~1 cm thick slice from the deepest part of the core was retrieved, freeze-dried, and analysed for radiocarbon dating (sample label G1-X\*).

### 2.3. Stratigraphic and micromorphological analysis

The geoarchaeological description was conducted according to sedimentological, pedological, and stratigraphic criteria (Goldberg et al., 2022) (see Table S1 in Supporting Material). Colours were codified using *Munsell® Soil Colour Charts* and determined on wet samples (*Munsell Soil Color Charts*, 2000). The Udden-Wentworth scale (1922) was used for characterizing the grain size of the sediments. The carbonate content in the sediments is based on the semiquantitative observation of the reaction to 10 % diluted HCl. Soil horizons and sediments were described following the FAO guidelines (2006). The symbols used for soil classification and horizon definition follow the criteria of Soil Taxonomy (IUSS Working Group WRB, 2015). Archaeological micromorphology was used to analyse the combined effects of geogenic, biogenic, and anthropogenic processes. Six sediment samples were prepared at the *Servizi per la Geologia* laboratory (Piombino, Italy) following the methodology reported in Murphy (1986), which includes dehydration, vacuum impregnation with polymerizing resins, cutting into centimetre-thick slabs, and final preparation of thin sections with a thickness of 25 µm and dimensions of 95 mm × 55 mm, without cover glass. The thin sections were analysed using a Prior MP3500A petrographic optical microscope, with plane polarized light (PPL) and cross polarized light (XPL) at 20x, 40x, 100x, and 400x magnifications. The nomenclature used for the description of the thin sections follows Stoops (2021) for the study of sediments and soils, while the interpretation of the components is mainly based on definitions by Nicosia and Stoops (2017) and Stoops et al. (2018) (see Table S1 in Supporting Material).

### 2.4. Radiocarbon dating

Charcoal samples from the 160.01 trench (n = 8), from OS (n = 9) and SS (n = 1) layers, together with C-PH and guano bat (G1-X\*) were sent to the Vilnius Radiocarbon Laboratories in Lithuania and analysed

using Accelerated Mass Spectrometry (AMS). Conventional Radiocarbon Ages (CRA) were calibrated using OxCal v4.4 (Bronk Ramsey, 2021) and the IntCal20 atmospheric curve (Reimer et al., 2020). Calibrated ages are reported in cal y BP or in CE for practicality.

## 2.5. Anthracology

Charcoal remains sent to radiocarbon dating were examined using an incident light microscope at magnifications of  $100 \times$ ,  $200 \times$ , and  $500 \times$ . Taxonomical identification was performed through comparison with standard wood atlases (Vernet et al., 2001; Abbate Edlmann et al., 1994; Schweingruber, 1990; Greguss, 1955). The excellent state of preservation allowed taxonomic determinations at the species or genus level, with botanical nomenclature following Pignatti (1982). In some instances, taxonomic designations were grouped according to anatomical type following Schweingruber (1990) and Vernet et al. (2001). For example, charcoal classified as "*Pinus sylvestris* type" may correspond to *Pinus sylvestris*, *Pinus nigra*, or *Pinus mugo/uncinata*, although charcoal analysis inherently presents challenges due to the absence of specific diagnostic key features.

## 2.6. Physical and chemical analysis

The pH measurements of the sediments and guano were carried out in all samples using a pH-Meter (Hanna Instruments – HI 2210), following the methodology reported in FAO (2021). Total organic carbon (TOC%) in the sediments was analysed using a Total Organic Carbon Analyzer (Model TOC-L, Shimadzu 5050A) following the manufacturer instructions.

X-ray powder diffraction patterns were recorded with conventional Bragg-Brentano geometry at 295 K, with a step size of  $0.05^\circ$  on a scale of  $5\text{--}145^\circ$  2 $\theta$  and a time of 500 s/step. An Empyrean diffractometer (Malvern Panalytical Ltd.) equipped with Bragg-Brentano HD incident optics,  $1/8^\circ$  divergence slit and copper X-ray tube (wavelength  $K\alpha$  1.5406 Å) at 40 kV and 40 mA was used. A hybrid 2D solid-state pixel detector PIXcel3D (255 active channels) was employed. The research of the constituting phases of the samples and a semiquantitative phase analysis by X-ray diffraction was performed using Sieve+® program within PDF-5+ data base.

The determination of trace elements (TE) and rare earth elements (REE) in the sediments and guano was carried out by acid digestion in a microwave oven, followed by inductively coupled plasma-mass spectrometry (ICP-MS) analysis. ICP-MS analysis was performed using an iCAP-RQ (Thermo Scientific). Further methodological details are reported in Supporting Material. A total of 33 elements were monitored, including trace elements (TE): Na, Mg, Al, K, Ca, Sc, Ti, V, Cr, Mn, Fe, Co, Ni, Cu, As, Sr, Y, Ba, Pb; and Rare Earth Elements (REE): La, Ce, Pr, Nd, Sm, Eu, Gd, Tb, Dy, Ho, Er, Tm, Yb, and Lu. All elements were acquired in triplicate and quantified by external calibration with standards prepared from multi-elemental solutions (Ultra Scientific). An on-line spike of Rh at  $10 \text{ ng mL}^{-1}$  was used as the internal standard. Accuracy was assessed through contextual mineralization and analysis of certified reference materials NIMT/UOE/FM/001 (peat) and BCR-667 (estuarine sediment).

The determination of faecal sterols and stanols in sediments and guano was carried out following the analytical method proposed by Battistel et al. (2015) and further modifications reported in Bortolini et al. (2024). GC-MS analysis was performed using a 7890A-GC system coupled with a 5975C MSD single quadrupole spectrometer. Additional details are reported in Supporting Material. A total of 10 sterols and stanols were analysed:  $5\beta$ -Cholestan- $3\beta$ -ol (coprostanol; CoP),  $5\beta$ -Cholestan- $3\alpha$ -ol (epi-coprostanol; e-CoP), Cholest-5en- $3\beta$ -ol (cholesterol; Chol),  $5\alpha$ -Cholestan- $3\beta$ -ol ( $5\alpha$ -cholestanol;  $5\alpha$ -Ch), 24-Methyl-cholest-5en- $3\beta$ -ol (campesterol; Camp), 24-Ethyl-Cholesta-5,22-en-dien- $3\beta$ -ol (stigmasterol; Stg-ol), 24-Ethyl-cholest-5en- $3\beta$ -ol ( $\beta$ -sitosterol;  $\beta$ -sito), 24-Ethyl- $5\beta$ -cholestan- $3\beta$ -ol ( $5\beta$ -stigmastanol;  $5\beta$ -Stg),

24-Ethyl- $5\beta$ -cholestan- $3\alpha$ -ol (epi- $5\beta$ -stigmastanol, e- $5\beta$ -Stg), 24-Ethyl- $5\alpha$ -cholestan- $3\beta$ -ol ( $5\alpha$ -stigmastanol;  $5\alpha$ -Stg). An adequate number ( $n = 5$ ) of procedural blanks were analysed.

## 2.7. Statistical analysis

The normality of the distributions was assessed using the Shapiro-Wilk test, while the presence of outliers was examined using the Dixon test. The means of the populations were compared using the Student t-test, the Welch t-test (for unequal variances), and the Mann-Whitney U test (for non-normally distributed populations). Principal component analysis was performed using trace elements and the sum of rare earth elements as z standardized variables. All statistical analyses were performed using R packages (R 4.4.3 version). The pH, TOC, PC1, PC2 and Pb distribution maps reported in Fig. 5 were obtained by linear interpolation of the punctual values. The cumulative probability density function in Fig. 7 is created by superposition of individual distributions for each  $^{14}\text{C}$  date.

## 3. Results

### 3.1. Trench 160.01

#### 3.1.1. Stratigraphy and micromorphology

SU-1 is a recent deposit of spoil material from the illegal excavation of the underlying units. The underlying SU-2 (see Fig. 2 and Table S2 in Supporting Material) is divided into two subunits (SU-2A and SU-2B).

SU-2A has a maximum thickness of 3 cm and corresponds to a trampled surface, which has compacted and imprinted a primary wavy lamellar microstructure on the top of unit SU-2B (see Fig. 3A and B). SU-2B is a paleosol (Ah) with a thickness of about 20 cm, characterized by anthropogenic components (carbon fragments, flint lithic industry, organic matter). At the microscopic level, it is characterized by a weakly developed subangular polyhedral microstructure with accommodated parallel and subvertical planar voids, and an open porphyric relative distribution. The micromass predominantly (80 %) consists of dark brown quartz silt-clay with mica-muscovite, feldspars and an undifferentiated b-fabric. The coarse mineral component ranges from very fine sand (125  $\mu\text{m}$ ) to subrounded granules (<5 mm). The mineral fraction consists almost entirely of local basalt and, to a lesser extent, angular reddish minerals and cryptocrystalline flint. Some flint fragments show signs of thermal alteration (i.e. crazing) (Angelucci, 2017). The only pedological features present are pedorelicts dispersed in the micromass with a chaotic distribution pattern. Rounded and subrounded forms, often of a nucleic type, are recognized, making up around 10 % of the micromass, formed around rock fragments (basalt, flint), as well as some matrix coatings on the coarse mineral fraction, indicating a rolling action of granules. Less common are brunified, non-brunified and rubified pedorelicts with lamellar subangular shapes (length 9 mm), along with pedofeatures consisting of rounded fragments of microlaminated clay coatings, remnants of ancient illuviation horizons. Organic matter is common and represented by pinpoint particles, fragments of decomposed herbaceous plant tissue that is partially burned and opaque (Herbaceous Partly Burnt, 10–200  $\mu\text{m}$ ). Charcoal and microcharcoal are common (5 %) and reach sizes of several millimetres (max. 8 mm). Well-represented are phosphatized bone fragments with subrounded or rounded edges, degraded by biological agents (>125  $\mu\text{m}$  < 2 mm, 2 %), likely ingested and excreted by meso- and macrofauna. Disorthic nodules typical of cryptocrystalline apatite are recognizable by their light-yellow colour in PPL and isotropic appearance in XPL.

SU-3 is a stratified deposit consisting of weakly clayey silt, non-calcareous, massive, and apedal (Fig. 3C and D). Thirteen lenticular subunits with wavy, abrupt boundaries and local hints of water-transported lamination were distinguished in the unit based on colorimetric analysis. The upper part of SU-3 displays post-depositional deformation in the form of load casts that create flame-like structures.

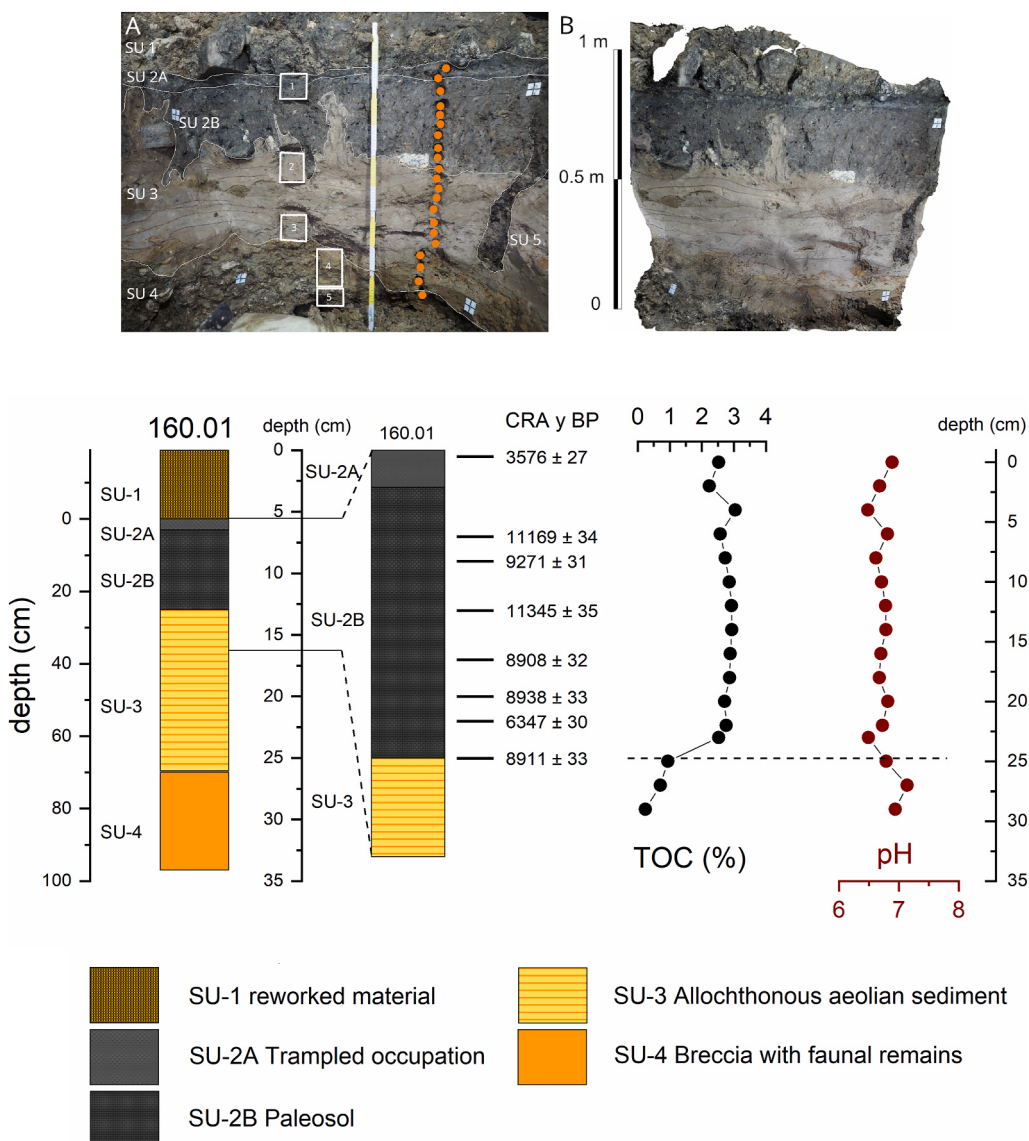


**Fig. 2.** A) Stratigraphic profile of trench 160.01 with stratigraphic units (SU), micromorphology samples (1–5) and in orange the sampling sequence for physical and chemical analyses, including radiocarbon data; B) orthophoto of the section of trench 160.01.A). (Below) Schematic representation of the stratigraphic units individuated in 160.01, including radiocarbon data (reported in CRA y BP), the TOC% and pH profiles covering SU-2 and part of SU-3.

These features develop when the denser sediments of Unit 2B sink into the underlying, less-dense, water-saturated Unit 3. The micromass is predominant (80–95 %) over the coarse fraction (>125 µm), and both show components and a g/f relative distribution similar to unit SU-2B. Unlike SU-2B, there is the development of polyconcave voids, locally organized into a vesicular microstructure, revealing evidence of the collapse of original voids due to water saturation. Some moldic voids of faunal remains are present. As in the upper unit, clayey pedorelicts (10 %, >250 µm < 2.5 mm) are common, including rare subrounded fragments of microlaminated clay coatings. The presence of clay intercalations and Fe-Mn oxide/hydroxide hypocoatings within the voids testifies to cycles of water saturation alternating with aerobic exposure. The organic fraction ranges from 2 to 5 % and it is represented by amorphous fine material and burnt plant matter. Charcoal and micro-charcoal fragments are poorly represented (2 %). Bone fragments have subrounded boundaries (>250 µm < 2.5 mm, 10 %) and show moderately Fe-Mn impregnations. Complete mineral dissolution of the mass is observed, with the replacement of secondary pseudomorphic phosphate minerals on the original bone tissue (Villagran et al., 2017).

Only the top portion of the underlying SU-4 was investigated (Fig. 3E

and F). It is a clast-supported breccia with abundant macrofaunal remains, mainly consisting of oolitic-bioclastic grainstone clasts (95 %) that are equant or platy in shape and exhibit chemically altered cortices (cortex). The coarse fraction also includes basalt grains (max. diameter 2.5 mm, 2 %) and cryptocrystalline flint, both showing evidence of crazing. In PPL, the cortex of the calcareous clasts features an internal exfoliation zone characterized by the complete or partial dissolution of ooids and bioclasts. The voids in the lower and upper portions of the cortex are filled with yellow phosphates. The microstructure is generally massive, tending toward planar lamination, with subvertical planar voids and polyconcave voids. Pedological features include Fe-Mn (hydr) oxide hypocoatings, phosphatic nodules, and discontinuous loose micrite infillings, derived from the partial dissolution of the calcareous clasts. Rounded and subrounded pedorelicts (10 %, >250 µm < 2.5 mm) are still present in the groundmass. The micromass has a granostriated b-fabric and constitutes a secondary fill closely resembling the overlying SU-3. Among the pedological features are those formed in hydromorphic conditions—such as Fe-Mn (hydr)oxygenate hypocoatings in voids and alteration films on bones. Under the microscope, a total loss of birefringence is observed in the bones. The state of preservation of the faunal

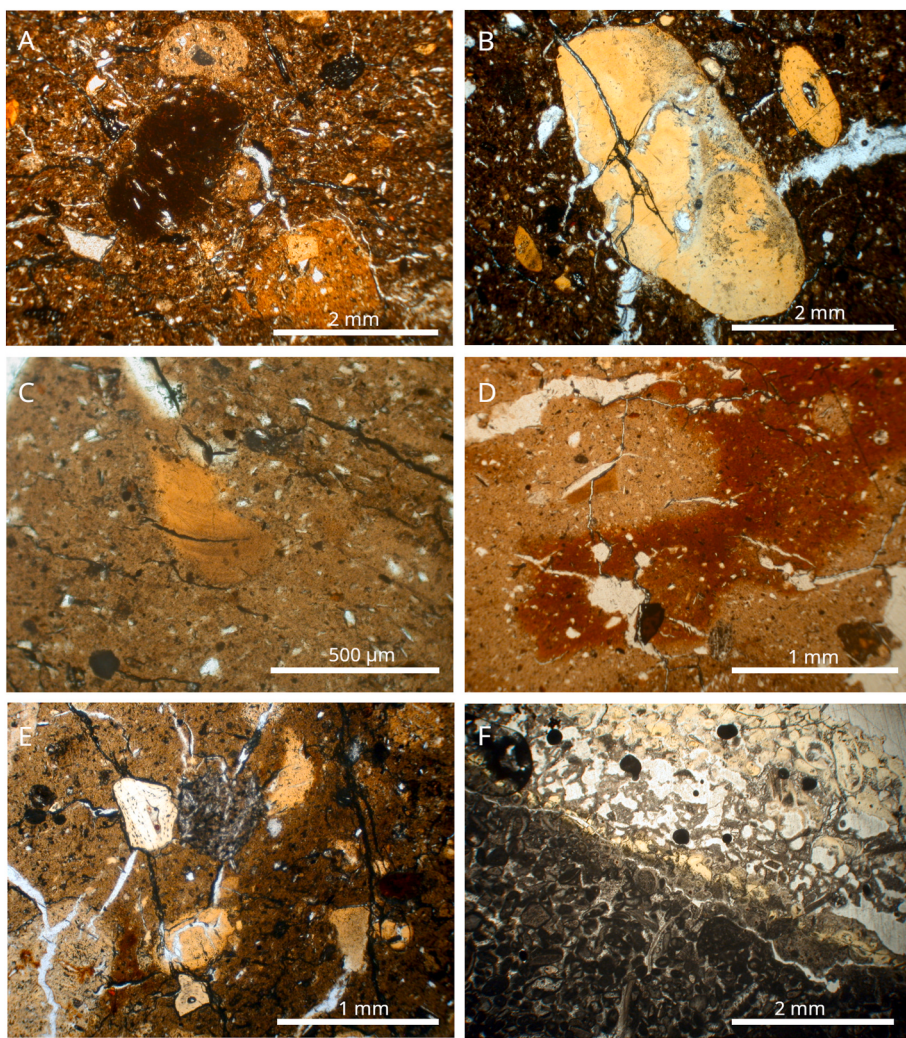


**Fig. 3.** A) SU 2B, rounded and subrounded rubified and brunified pedorelicts (PPL), 20x; B) SU 2B, rounded and subrounded phosphatized bone fragments (PPL), 20x; C) SU 3, subangular fragment of microlaminated clay coating (PPL), 20x; D) SU 3, impregnative pedofeatures with high concentration of Fe oxides (probably hematite) (PPL), 40x; E) SU 4, groundmass with partially phosphatized sub-rounded bone fragments and rounded pedorelicts (PPL), 20x; F) SU 4, cortex of the calcareous clasts characterized by the complete or partial dissolution of ooids and bioclasts. The voids in the lower and upper portions of the cortex are filled with yellow phosphates. (PPL), 40x.

remains suggests dissolution processes that removed organic material from the bones, leading to their complete or partial dissolution. Given that SU-4 was only partially exposed; a comprehensive analysis of this unit will be presented in a subsequent study. Consequently, the current paper focuses on stratigraphic units SU-2 and SU-3.

### 3.1.2. Charcoal

The charcoal samples ( $n = 8$ ) collected at different depths in trench 160.01 were radiocarbon dated (see Table 1). As reported in Table 1, calibrated radiocarbon ages range from ~4000 cal y BP to ~13,000 cal y BP, with ages between ~10,000 and ~11,000 cal y BP being predominant (4 out of 8 samples). Although these four samples might derive from the fragmentation of a single charcoal piece, the size of each fragment (~1 cm) as well as the wide depth range suggest that they are independent. Their independency is supported by the results of the anthracological investigation as these charcoal fragments derived from different wood taxa, mainly attributed to broad-leaved deciduous trees such as *Quercus* and *Corylus avellana* (see afterwards and Table 1). As shown in Fig. 2, the eight radiocarbon ages along the sedimentary profile suggest the absence of a well-defined chronological sequence, indicating that the depositional process was not unperturbed in SU-2. This occurrence may be related to sediment reworking by faunal or

anthropogenic activities, associated with the frequentation of the cave. A residual “old-wood” effect (i.e. fuelwood from long-dead logs collected outside the cave) cannot be entirely excluded. However, such a mechanism would not plausibly generate the multi-millennial spread observed. The offsets of several thousand years would require people to burn centuries to millennia old wood, which seems to be unlikely. We therefore view post-depositional mixing, rather than fuel age, as the primary cause of the mixed sequence. However, despite the absence of a well-defined chronology, we can hypothesize that SU-2 began to form during the glacial/post-glacial transition, while SU-3 broadly corresponds to an older phase of the Late Pleistocene, as supported by the recovery of fossil bones attributed to *U. spelaeus* in the underlying SU-4 (Ghezzo et al. in preparation). The C-PH sample found in the inner part of the cave, near trench 160.01, tentatively interpreted as deriving from a structural vertical wooden element, dates to ~12,700 cal y BP. The corresponding taxonomic analysis of the charcoal sample identified the wood as a conifer of *P. sylvestris* type (Table 1). It is worth noting that the charcoal fragments identified as Conifer or categorised as *P. sylvestris* type in the C-160.01.x dating sequence show a chronological interval consistent with C-PH, thus appearing to be contemporary to the wood in posthole and resulting the older charred remains of the trench 160.01.

**Table 1**

Conventional and calibrated radiocarbon ages of charcoal and guano samples from Cave A. Calibration was carried out using OxCal v4.4 and the IntCal20 atmospheric curve.

| Label       | Material  | Site   | Unit                | CRA y BP   | Cal y BP (2σ)                                  | Wood Taxa                     |
|-------------|-----------|--------|---------------------|------------|--|-------------------------------|
| C-160.01.21 | Charcoal  | 160.01 | SU-2A               | 3576 ± 27  | 3934-3827 (80.6 %)<br>3974-3943 (10.1 %)       | <i>Corylus avellana</i>       |
| C-160.01.27 | Charcoal  | 160.01 | SU-2B               | 11169 ± 34 | 13169-13061 (93.6 %)<br>13025-13006 (1.9 %)    | Conifer                       |
| C-160.01.29 | Charcoal  | 160.01 | SU-2B               | 9271 ± 31  | 10570-10339 (91.1 %)<br>10322-10301 (4.3 %)    | <i>Ulmus</i>                  |
| C-160.01.33 | Charcoal  | 160.01 | SU-2B               | 11345 ± 35 | 13307-13166 (95.4 %)                           | <i>P. sylvestris</i> type     |
| C-160.01.37 | Charcoal  | 160.01 | SU-2B               | 8908 ± 32  | 10183-9907 (95.4 %)                            | deciduous <i>Quercus</i> type |
| C-160.01.40 | Charcoal  | 160.01 | SU-2B               | 8938 ± 33  | 10086-9910 (55.4 %)<br>10203-10111 (40.0 %)    | <i>Corylus avellana</i>       |
| C-160.01.42 | Charcoal  | 160.01 | SU-2B               | 6347 ± 30  | 7328-7242 (67.4 %)<br>7217-7167 (26.2 %)       | cf. <i>Salix</i>              |
| C-160.01.45 | Charcoal  | 160.01 | SU-2: SU-3 boundary | 8911 ± 33  | 10186-9907 (95.4 %)                            | Fagaceae                      |
| C-PH        | Charcoal  | –      | –                   | 10868 ± 34 | 12740-12836 (95.4 %)                           | <i>P. sylvestris</i> type     |
| C-OS-I      | Charcoal  | I      | OS                  | 11307 ± 35 | 13254-13116 (86.0 %)<br>13300-13267 (9.5 %)    | Conifer                       |
| C-OS-II     | Charcoal  | II     | OS                  | 11576 ± 42 | 13509-13335 (92.4 %)<br>13574-13558 (4 %)      | <i>P. sylvestris</i> type     |
| C-SS-II     | Charcoal  | II     | SS                  | 11345 ± 42 | 13314-13161 (94.4 %)<br>13134-13126 (1.1 %)    | <i>P. sylvestris</i> type     |
| C-OS-III    | Charcoal  | III    | OS                  | 19619 ± 72 | 23622-23355 (63.5 %)<br>23823-23678 (32.2 %)   | <i>Picea/Larix</i>            |
| C-OS-IV     | Charcoal  | IV     | OS                  | 9205 ± 40  | 10441-10248 (82.1 %)<br>10497-10459 (13.4 %)   | Indeterminable                |
| C-OS-V      | Charcoal  | V      | OS                  | 9417 ± 38  | 10752-10561 (93.3 %)<br>10536-10516 (2.2 %)    | <i>Corylus avellana</i>       |
| C-OS-VI     | Charcoal  | VI     | OS                  | 9454 ± 39  | 10782-10575 (89.6 %)<br>11000-10973 (4.0 %)    | <i>Alnus</i>                  |
| C-OS-VII    | Charcoal  | VII    | OS                  | 9029 ± 35  | 10246-10167 (94.5 %)                           | <i>Euonymus</i>               |
| C-OS-VIII   | Charcoal  | VIII   | OS                  | 262 ± 29   | 1620-1672 CE (53.0 %)<br>1516-1591 CE (31.1 %) | cf. <i>Alnus</i>              |
| C-OS-X      | Charcoal  | X      | OS                  | 131 ± 29   | 1799-1942 CE (64.4 %)<br>1675-1744 CE (26.9 %) | Hardwood/Node                 |
| G1-X*       | Bat guano | Guano  | –                   | –255 ± 28  | 2011-2014 CE (75.9 %)<br>1955-1956 CE (18.4 %) | –                             |

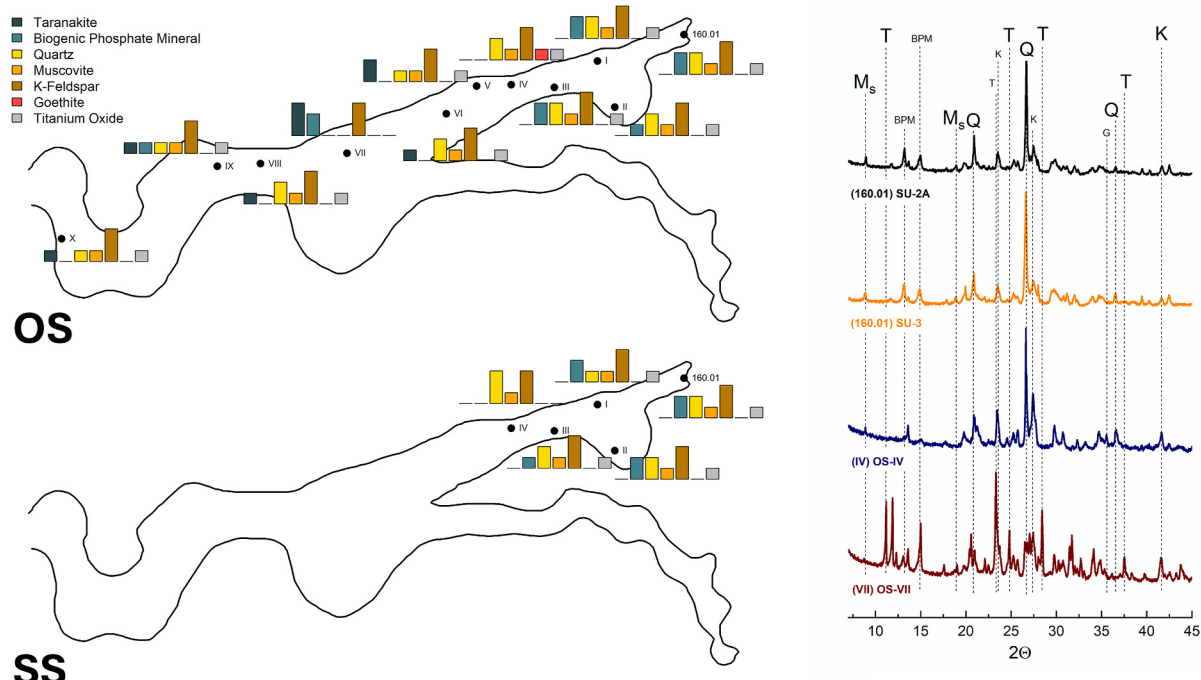


**Fig. 4.** Representative XRD spectra (i.e. OS-II, OS-IV and OS-VII) (right) and spatial phase distribution in OS-type and SS-type sediments (left). The bar plot represents the approximate abundance of each crystalline phase on a scale from 0 to 3, where: 0 indicates non-detectable levels; 1 corresponds to a detectable abundance of less than 15 %; 2 represents values between 15 and 30 %; and 3 corresponds to values between 30 and 45 %. The XRD spectra include the following phases: Taranakite (T), Biogenic Phosphate Minerals (BPM), K-Feldspar Polymorph (K; including sandine and microcline) Muscovite (Ms), Quartz (Q) and Goethite (G).

### 3.1.3. XRD analysis

A representative X-ray diffraction pattern from SU-2 (Fig. 4, upper right) shows the presence of quartz, muscovite, and K-feldspar together with a suite of biogenic phosphate minerals (BPMs). The spectrum of SU-3 (not shown) is essentially identical to the SU-2 spectrum, confirming that the two units share the same mineral assemblage. Consistent with micromorphological observations, no carbonate phases were detected in either unit, despite the extensive carbonate crust on the cave ceiling.

The abundance of K-feldspar, muscovite and quartz points to an allochthonous sediment source, deriving from the plateau outside the cave, although it cannot be ruled out that part of the quartz may derive from the alteration of the paleokarstic infill at the basaltic dyke, as described by Gonzato et al. (2017), which consists of laminated limonitic silt and breccia, cemented by microcrystalline quartz.

XRD spectra from 160.01 sediments also exhibit weak peaks attributable to BPMs formed by (i) direct guano degradation and/or (ii) reaction between guano-derived phosphorous-rich leachates and aluminium in the host clay minerals (Onac, 2012), also found in other cave environments (Frost et al., 2011; Miko et al., 2001; Fiore and Laviano, 1991). These spectra are consistent with brushite and/or monetite, while other biogenic phosphates such as ardeelite, withlockite and leucophosphate can be reasonably be excluded. However, the complex matrix and the relatively low abundance precludes unambiguous phase identification. Therefore, these phosphorous-bearing phases are hereinafter collectively referred to as biogenic phosphorous minerals. The contextual evidence strongly implicates bat guano as the principal source of both phosphorous and ammonium.

### 3.1.4. Chemical analysis

The pH profile of the sedimentary sequence is reported in Fig. 2. As shown, pH values ranged from 6.5 to 7.1, with a mean value of 6.8 (0.2) (standard deviation in brackets). The pH is essentially neutral or slightly acidic, and almost constant throughout the record, without showing any significant difference between SU-2 and SU-3, as demonstrated by the Student t-test ( $p$ -value = 0.42). Conversely, total organic carbon showed significantly higher values ( $p$ -value = 0.0055) in SU-2 (2.7 (0.2) %) compared to SU-3 (0.6 (0.4) %), indicating that the sediment in SU-2 is approximately five times more enriched in organic matter. Although not reported, the concentration of inorganic carbon is below the limit of

detection ( $\text{LoD} = 0.01\%$ ), indicating that the presence of carbonates is negligible in both stratigraphic units. The lack of carbonates is consistent with XRD analysis and the micromorphological investigation.

Since the only variability along the sedimentary record was observed between the stratigraphic units SU-2 and SU-3, the determination of major and trace elements was carried out in the combined samples SU-2A, SU-2B and SU-3 (Table 2). The ratio between all the elements of the two units was calculated associating a confidence interval determined by the propagation of the uncertainty (~15 % on average). Therefore, elemental ratios that fell in the range 0.7–1.3 were considered as not significant. The elemental ratios between SU-2A and SU-2B showed that all the elemental ratios are included in the range 0.7–1.3, suggesting the absence of any significant differences between the elemental composition of SU-2A and SU-2B. Conversely, SU-3 compared to SU-2 (averaging SU-2A and SU-2B) showed a significant enrichment in Mn (1.4), Rb (1.4), Mg (1.5) and REE (2.4, on average) as well as a depletion in Cu (0.4) and Ag (0.6).

The organic fraction of the sediment was analysed for faecal sterols and stanols in sample SU-2B and SU-3 (Table 3). As reported, SU-2B and SU-3 showed a different compositional faecal sterols pattern, where coprostanol is more abundant in SU-2B, while  $\beta$ -sitosterol prevails in SU-3. Moreover, the steroid composition in both units consistently deviates from the guano sample (Table 3). In the sediment, we observed a larger presence of zoo 5 $\beta$ -stanols in SU-2B while, in SU-3, the larger increase in  $\beta$ -sitosterol is not followed by the increase in cholesterol. The faecal sterol concentrations and pattern deviate from guano samples, where sterols (mainly cholesterol and  $\beta$ -sitosterol) are predominant.

## 3.2. Interphases along the transect I-X

### 3.2.1. Charcoal and anthracology

The rich organic sediment found in OS samples is characterized by a larger load of charcoal fragments, similarly to SU-2. Conversely, in SS only a single fragment, approximately 2 mm in size (C-SS-II), was found. Although it is difficult to robustly quantify the abundance of charcoal in the sediment, due to possible post-depositional fragmentation and/or inhomogeneous accumulation, we observed a greater abundance (approximately 5–10 cm<sup>-3</sup>) and larger maximum size (~3–4 mm) of charcoal fragments in the transect I-VI and in the trench 160.01,

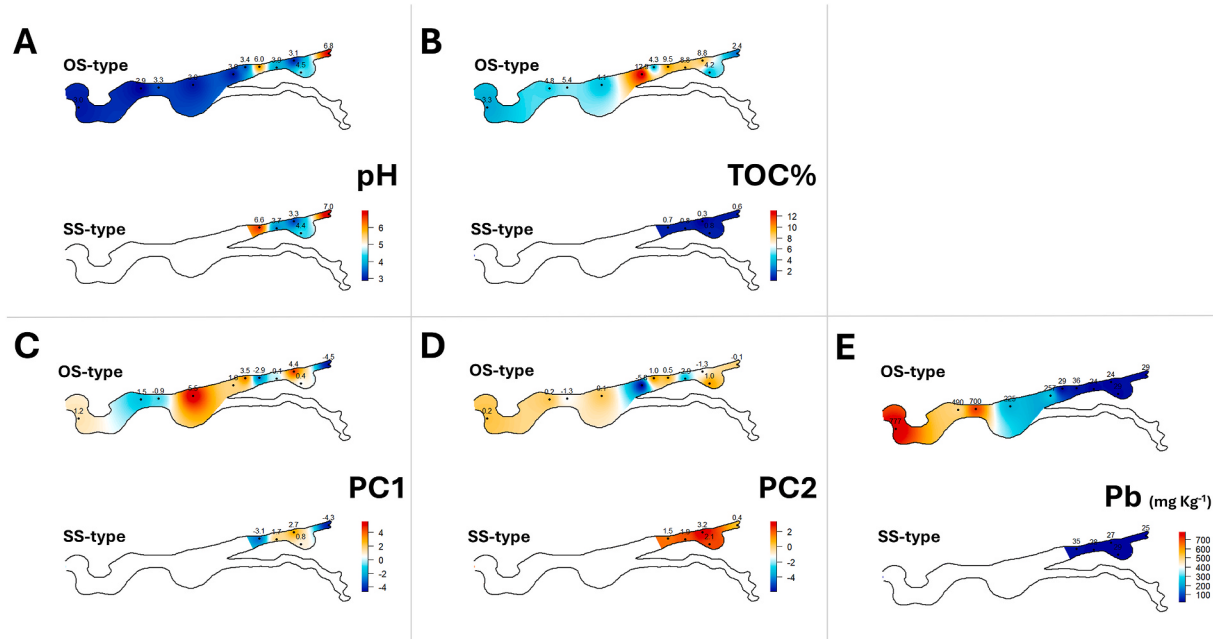


**Fig. 5.** pH (A), TOC% (B), PC1 (C), PC2 (D) and Pb (D) in 160.01 and I-IX sediments. OS-type (top) and in SS-type (bottom) in each figure.

**Table 2**

Bulk chemical composition of sediments from stratigraphic units SU-2A, SU-2B, and SU-3 in trench 160.01; upper (OS) and lower (SS) layers along the transect; and ochre and bat-guano samples. Major elements (Al, Fe, Mg, Ca, Na, K, Mn, Ti) are reported in g kg<sup>-1</sup>. Total organic carbon (TOC) and total inorganic carbon (TIC) are reported in wt%. Trace elements and rare-earth elements (REE) are reported in mg kg<sup>-1</sup>. Values below the limit of detection are reported as < lod; not analysed is indicated by “-”.

|     | SU-2A | SU2-B | SU-3  | OS-I  | SS-I  | OS-II | SS-II | OS-III | SS-III | OS-IV | SS-IV | OS-V  | OS-VI | OS-VII | OS-VIII | OS-IX | OS-X  | Ochre | Bat guano |
|-----|-------|-------|-------|-------|-------|-------|-------|--------|--------|-------|-------|-------|-------|--------|---------|-------|-------|-------|-----------|
| Al  | 23.6  | 25.8  | 31.5  | 5.5   | 7.4   | 10.6  | 9.2   | 9.3    | 9.6    | 14.8  | 15.2  | 8.5   | 4.6   | 4.2    | 10.8    | 11.6  | 6.4   | 7.5   | 0.7       |
| Fe  | 32.2  | 31.4  | 29.5  | 23.3  | 25.6  | 33.0  | 34.4  | 32.6   | 31.6   | 86.7  | 54.0  | 41.9  | 28.0  | 18.5   | 33.0    | 47.9  | 32.7  | 334   | 0.34      |
| Mg  | 557   | 535   | 814   | 51    | 78    | 110   | 105   | 137    | 89     | 325   | 261   | 37    | 97    | 129    | 164     | 108   | 98    | 2900  | 3700      |
| Ca  | 15.2  | 17.6  | 19.8  | 1.2   | 1.1   | 2.6   | 1.7   | 2.4    | 1.4    | 2.9   | 3.8   | 0.7   | 1.8   | 1.2    | 2.9     | 2.5   | 2.2   | 55    | 5.4       |
| Na  | 4.8   | 5.1   | 4.7   | 2.0   | 2.7   | 3.0   | 3.9   | 2.4    | 3.3    | 3.7   | 4.2   | 2.3   | 1.8   | 1.0    | 4.4     | 3.0   | 5.1   | 0.2   | 1.0       |
| K   | 32    | 30    | 36    | 28    | 38    | 33    | 38    | 24     | 34     | 30    | 35    | 32    | 22    | 51     | 33      | 37    | 38    | 1.0   | 5.7       |
| Mn  | 0.353 | 0.278 | 0.452 | 0.090 | 0.122 | 0.244 | 0.250 | 0.202  | 0.243  | 0.169 | 0.330 | 0.194 | 0.083 | 0.036  | 0.129   | 0.105 | 0.112 | 0.069 | 0.110     |
| Ti  | 14.7  | 15.0  | 13.1  | 9.2   | 16.8  | 15.1  | 15.1  | 11.6   | 14.4   | 17.1  | 17.2  | 12.1  | 8.3   | 16.2   | 15.0    | 18.3  | 14.5  | 0.5   | 0.04      |
| TOC | 2.6   | 2.9   | 0.7   | 8.8   | 0.3   | 4.2   | 0.8   | 8.8    | 0.8    | 9.5   | 0.7   | 4.3   | 12.9  | 4.1    | 5.4     | 4.8   | 3.3   | -     | -         |
| TIC | < lod  | < lod  | < lod | < lod | < lod | < lod | < lod  | < lod   | < lod | < lod | -     | -         |
| pH  | 6.8   | 6.8   | 6.8   | 3.1   | 3.3   | 4.5   | 4.4   | 3.9    | 3.7    | 6.0   | 6.6   | 3.4   | 3.0   | 3.0    | 3.3     | 2.9   | 3.0   | -     | 3.2       |
| Li  | 11.9  | 21.6  | 11.9  | 2.9   | 13.8  | 6.8   | 10.3  | 18.3   | 8.6    | 8.2   | 12.4  | 3.6   | 6.0   | 0.5    | 10.5    | 6.2   | 7.4   | 3.1   | < lod     |
| Sc  | 12.4  | 13.0  | 12.7  | 1.7   | 2.7   | 5.2   | 3.7   | 5.0    | 3.4    | 7.6   | 8.1   | 2.3   | 3.4   | 2.7    | 5.9     | 10.4  | 2.9   | 9.9   | < lod     |
| V   | 180   | 187   | 163   | 128   | 198   | 181   | 195   | 157    | 173    | 321   | 244   | 188   | 166   | 146    | 187     | 236   | 138   | 560   | 3.4       |
| Cr  | 325   | 285   | 284   | 215   | 297   | 295   | 282   | 250    | 251    | 353   | 375   | 240   | 236   | 291    | 301     | 425   | 237   | 13    | < lod     |
| Co  | 14    | 16    | 12    | 16    | 6     | 12    | 11    | 60     | 9      | 17    | 14    | 9     | 80    | 10     | 30      | 22    | 15    | 2.5   | < lod     |
| Ni  | 67    | 65    | 50    | 22    | 16    | 31    | 36    | 54     | 33     | 66    | 57    | 26    | 104   | 24     | 54      | 42    | 34    | 84    | 2.1       |
| Cu  | 392   | 294   | 159   | 270   | 88    | 371   | 175   | 994    | 152    | 292   | 225   | 172   | 1806  | 402    | 683     | 1274  | 511   | 14    | 740       |
| Zn  | 523   | 565   | 638   | 158   | 179   | 442   | 463   | 376    | 396    | 276   | 373   | 216   | 290   | 84     | 262     | 273   | 427   | 96    | < lod     |
| As  | 12    | 13    | 10    | 8     | 6     | 8     | 8     | 14     | 7      | 92    | 35    | 27    | 9     | 6      | 19      | 11    | 8     | 615   | < lod     |
| Rb  | 23.1  | 18.7  | 29.8  | 29.8  | 33.2  | 30.5  | 36.5  | 19.7   | 36.1   | 17.1  | 23.2  | 28.1  | 16.4  | 31.0   | 19.0    | 25.8  | 37.3  | 8.2   | 1.6       |
| Sr  | 111   | 107   | 99    | 26    | 29    | 36    | 33    | 38     | 30     | 48    | 62    | 18    | 27    | 21     | 60      | 114   | 48    | 54    | 100       |
| Y   | 25.7  | 31.2  | 88.4  | 0.5   | 0.1   | 0.7   | 0.2   | 1.5    | 0.1    | 2.5   | 1.9   | 0.1   | 3.9   | 0.7    | 1.7     | 2.0   | 1.1   | 31    | < lod     |
| Mo  | 0.33  | 0.41  | 0.33  | 0.30  | 0.19  | 1.62  | 0.72  | 1.45   | 0.91   | 1.07  | 0.33  | 0.48  | 2.23  | 0.80   | 1.02    | 0.47  | 1.17  |       |           |
| Ag  | 0.18  | 0.09  | 0.12  | 0.15  | 0.12  | 0.21  | 0.14  | 0.39   | 0.06   | 0.19  | 0.18  | 0.16  | 0.62  | 0.24   | 0.86    | 0.17  | 0.26  | < lod | < lod     |
| Ba  | 526   | 422   | 339   | 179   | 340   | 300   | 338   | 257    | 300    | 306   | 586   | 151   | 167   | 129    | 329     | 475   | 437   |       |           |
| Pb  | 29    | 28    | 25    | 24    | 27    | 29    | 29    | 24     | 28     | 36    | 35    | 29    | 257   | 225    | 700     | 490   | 777   | 65    | 2         |
| La  | 9.2   | 9.7   | 38.7  | 0.45  | 0.02  | 0.09  | 0.05  | 0.36   | 0.04   | 2.05  | 0.39  | 0.02  | 1.34  | 0.35   | 0.43    | 0.89  | 0.20  | 23.6  | 0.28      |
| Ce  | 22.4  | 23.2  | 63.7  | 2.9   | 0.27  | 0.38  | 0.21  | 1.1    | 0.11   | 3.4   | 2.1   | 0.10  | 3.4   | 1.9    | 2.2     | 2.6   | 0.9   | 21.0  | 0.49      |
| Pr  | 3.3   | 3.5   | 9.4   | 0.16  | 0.02  | 0.05  | 0.03  | 0.18   | 0.02   | 0.53  | 0.21  | 0.01  | 0.57  | 0.24   | 0.17    | 0.28  | 0.08  | 6.89  | 0.11      |
| Nd  | 15.8  | 17.8  | 49.4  | 1.59  | 0.12  | 0.28  | 0.12  | 0.83   | 0.09   | 1.94  | 1.24  | 0.06  | 2.03  | 1.43   | 1.08    | 1.34  | 0.46  | 29.6  | 0.30      |
| Sm  | 4.4   | 4.8   | 10.3  | 0.28  | 0.06  | 0.13  | 0.07  | 0.34   | 0.06   | 0.48  | 0.44  | 0.02  | 0.54  | 0.47   | 0.37    | 0.41  | 0.21  | 6.2   | < lod     |
| Eu  | 1.5   | 1.7   | 3.1   | 0.08  | 0.03  | 0.05  | 0.04  | 0.12   | 0.03   | 0.18  | 0.16  | 0.02  | 0.20  | 0.14   | 0.14    | 0.15  | 0.09  | 1.3   | < lod     |
| Gd  | 5.1   | 5.8   | 13.2  | 0.22  | 0.05  | 0.15  | 0.05  | 0.40   | 0.04   | 0.49  | 0.50  | 0.02  | 0.77  | 0.45   | 0.47    | 0.51  | 0.23  | 5.5   | < lod     |
| Tb  | 0.80  | 0.90  | 1.92  | 0.04  | 0.01  | 0.03  | 0.01  | 0.09   | 0.01   | 0.09  | 0.10  | 0.01  | 0.16  | 0.08   | 0.10    | 0.11  | 0.05  | 0.80  | < lod     |
| Dy  | 5.2   | 5.5   | 11.1  | 0.24  | 0.06  | 0.26  | 0.08  | 0.67   | 0.06   | 0.54  | 0.65  | 0.03  | 1.26  | 0.45   | 0.65    | 0.76  | 0.35  | 5.0   | < lod     |
| Ho  | 1.0   | 1.2   | 2.5   | 0.04  | 0.01  | 0.06  | 0.02  | 0.15   | 0.01   | 0.11  | 0.13  | 0.01  | 0.29  | 0.08   | 0.14    | 0.16  | 0.08  | 0.93  | < lod     |
| Er  | 3.0   | 3.2   | 6.8   | 0.13  | 0.04  | 0.20  | 0.06  | 0.47   | 0.05   | 0.31  | 0.37  | 0.02  | 0.95  | 0.22   | 0.40    | 0.49  | 0.23  | 2.9   | < lod     |
| Tm  | 0.42  | 0.43  | 0.91  | 0.02  | 0.01  | 0.03  | 0.01  | 0.07   | 0.01   | 0.05  | 0.06  | 0.004 | 0.15  | 0.03   | 0.06    | 0.08  | 0.04  | 0.42  | < lod     |
| Yb  | 2.4   | 2.8   | 5.3   | 0.15  | 0.04  | 0.24  | 0.09  | 0.53   | 0.06   | 0.32  | 0.39  | 0.03  | 0.98  | 0.20   | 0.41    | 0.53  | 0.27  | 2.6   | < lod     |
| Lu  | 0.35  | 0.38  | 0.75  | 0.02  | 0.01  | 0.04  | 0.02  | 0.08   | 0.01   | 0.05  | 0.06  | 0.01  | 0.15  | 0.03   | 0.06    | 0.07  | 0.04  | 0.44  | < lod     |
| REE | 74.9  | 80.9  | 217.1 | 6.3   | 0.7   | 2.0   | 0.9   | 5.4    | 0.6    | 10.5  | 6.8   | 0.4   | 12.8  | 6.1    | 6.7     | 8.4   | 3.3   | 107   | 1.2       |

**Table 3**  
Faecal steroids composition of the 160.01 (SU-2B and SU3), OS, SS and bat guano samples. In detail: Coprostanol (CoP), epi-Coprostanol (e-CoP), Cholesterol (Chol), 5 $\alpha$ -cholestane (5 $\alpha$ -Ch), 5 $\beta$ -stigmastanol (5 $\beta$ -Stg), epi-5 $\beta$ -stigmastanol (e-5 $\beta$ -Stg), Camposterol (Camp), Stigmasterol (Sig-ol),  $\beta$ -sitosterol (Sig-ol), 5 $\alpha$ -Sitostanol (5 $\alpha$ -Sitg).

|                      | SU-2B              | SU-3 | OS-I | SS-I | OS-II | SS-II | OS-III | SS-III | OS-IV | SS-IV | OS-V | OS-VI | OS-VII | OS-VIII | OS-IX | OS-X | Bat guano |        |
|----------------------|--------------------|------|------|------|-------|-------|--------|--------|-------|-------|------|-------|--------|---------|-------|------|-----------|--------|
| CoP                  | ng g <sup>-1</sup> | 800  | 10   | 490  | 65    | 146   | 16     | 296    | 27    | 85    | 3    | 69    | 856    | 4       | 13600 | 57   | 16        | 135    |
| e-CoP                | "                  | 42   | <lod | 25   | 12    | 9     | <lod   | 11     | 2     | 10    | <lod | 21    | 222    | 2       | 4484  | 68   | 2         | 244    |
| Chol                 | "                  | 131  | 46   | 2800 | 170   | 290   | 211    | 275    | 817   | 241   | 480  | 488   | 10     | 6600    | 997   | 53   | 62000     |        |
| 5 $\alpha$ -Ch       | "                  | 56   | 14   | 237  | 9     | 29    | 4      | 46     | 30    | 18    | <lod | 101   | 234    | 1       | 333   | 54   | 132       | 5360   |
| 5 $\beta$ -Stg       | "                  | <lod | <lod | 107  | <lod  | 2     | 133    | 1      | <lod  | 2     | 232  | 119   | <lod   | <lod    | 52    | 7    | 91        |        |
| e-5 $\beta$ -Stg     | "                  | <lod | <lod | 53   | <lod  | 29    | <lod   | 185    | 2     | 142   | <lod | 192   | 103    | 1       | 2360  | 51   | 12        | 78     |
| Camp                 | "                  | 23   | <lod | 45   | <lod  | 3     | 47     | 14     | <lod  | 20    | 115  | 211   | 10     | 1202    | <lod  | 14   | 5420      |        |
| Sig-ol               | "                  | 53   | <lod | 1608 | <lod  | <lod  | <lod   | 2055   | <lod  | 53    | 42   | 138   | 611    | <lod    | 53    | 53   | 3014      |        |
| $\beta$ -sitio       | "                  | 440  | 903  | 1500 | 185   | 88    | 27     | 668    | 218   | 66    | 235  | 1610  | 397    | 742     | 10750 | 1166 | 447       | 23300  |
| 5 $\alpha$ -Sitg     | "                  | 81   | 54   | 102  | 17    | 82    | 2      | 68     | 7     | 26    | 1    | 533   | 1      | 45      | 1585  | 77   | 76        | 1536   |
| $\Sigma$             | kg g <sup>-1</sup> | 1.61 | 1.11 | 5.2  | 0.61  | 2.28  | 0.26   | 1.73   | 1.12  | 2.64  | 0.27 | 3.41  | 2.67   | 0.95    | 41.5  | 2.52 | 0.81      | 101.18 |
| % sterol             |                    | 0.40 | 0.93 | 0.83 | 0.66  | 0.87  | 0.91   | 0.57   | 0.94  | 0.89  | 0.98 | 0.66  | 0.43   | 0.94    | 0.46  | 0.86 | 0.70      | 0.93   |
| % 5 $\beta$ stanol   |                    | 0.51 | 0.01 | 0.11 | 0.30  | 0.08  | 0.07   | 0.36   | 0.03  | 0.09  | 0.02 | 0.15  | 0.49   | 0.01    | 0.49  | 0.09 | 0.05      | 0.01   |
| % 5 $\alpha$ -stanol |                    | 0.08 | 0.06 | 0.07 | 0.04  | 0.05  | 0.02   | 0.07   | 0.03  | 0.02  | 0.02 | 0.19  | 0.09   | 0.05    | 0.05  | 0.05 | 0.26      | 0.07   |
| $\beta$ -sitio: Chol |                    | 3.4  | 20   | 0.5  | 1.1   | 0.3   | 0.1    | 2.4    | 0.3   | 0.3   | 0.3  | 18    | 3.4    | 0.8     | 74    | 1.6  | 1.2       | 8.4    |

compared to VII-X, where charcoal fragments were less abundant (~1–3 cm<sup>-3</sup>) and smaller in size (<1–2 mm).

The radiocarbon dating of 10 charcoal fragments collected along the transect (see Table 1) ranged from ~23,500 cal y BP (C-OS-III) to 1675–1942 CE (C-OS-X). Notably, the more recent fragments (i.e. younger than the 16th century CE) were found in transect VIII-X where the deposit is characterized by smaller and less abundant charcoal.

The oldest wood (C-OS-III) was identified as being from a conifer of the genus *Picea/Larix* (~23,500 cal y BP). Subsequently, two fragments dated between 13,500 and 13,100 cal y BP were attributed to Conifer and *P. sylvestris* type, contemporaneous with the conifer samples from trench 160.01 and the finds from posthole C-PH. Finally, three samples attributed to broadleaved deciduous trees (*Alnus*, *C. avellana* and *Euonymus* respectively) are dated between 11,000 and 10,200 cal y BP, similar to the broadleaved charcoal found in trench 160.01 (Table 1).

Interestingly, 14 out of 19 (~74 %) charcoal fragments (including the samples from trench 160.01 and C-PH) fall within the range of 9700–13,600 cal y BP.

### 3.2.2. XRD analysis

XRD analysis of the sediments along transect I–X revealed significant similarities among the deposits (see Fig. 4). Where both OS and the corresponding SS were sampled, the sediment from the two stratigraphic units exhibit essentially identical mineral assemblages, mirroring the pattern previously observed in trench 160.01 for units SU-2 and SU-3. K-feldspar minerals are ubiquitous, suggesting a sustained influx of allochthonous material throughout the cave. Biogenic phosphorous minerals (BPMs) are widespread; in several samples, particularly those from section B-C (Fig. 1), XRD unambiguously identifies taranakite [K<sub>3</sub>Al<sub>5</sub>(HPO<sub>4</sub>)<sub>6</sub>(PO<sub>4</sub>)<sub>2</sub>·18H<sub>2</sub>O], while other BPMs (i.e. brushite and/or monetite) are less abundant. The formation of taranakite through the interaction between bat guano leachates and Al-bearing minerals in cave environments is well documented (Onac, 2012; Fiore and Laviano, 1991; Frost et al., 2011). Because taranakite is stable under acidic, persistently wet and cool conditions (Frost et al., 2011), its absence – or at least much lower abundance – in section C-D (Fig. 1), may derive from locally less persistent wet conditions and/or a reduced guano load. On the other hand, the higher pH and the lower persistent humidity along this section are consistent with the formation of biogenic phosphates such as brushite and/or monetite (Sokol et al., 2022).

Sample SS-VII constitutes an outlier. Quartz and muscovite were not detected by XRD, mostly plausibly because their diffraction peaks are masked by the high taranakite content. Finally, goethite, which was identified in the ochre XRD spectrum (see Fig. S1 in Supporting Material), was only slightly present, but detectable, in sample SS-IV, which lies close to the ochre vein and is characterized by a higher pH (see the following paragraph).

### 3.2.3. Chemical analysis

The pH of the sediments collected in OS and SS along the transect generally differs from the values obtained in the trench 160.01. The pH values determined in the transect samples were generally more acidic, ranging from 2.9 to 4.5 (mean 3.5 ± 0.6), excepting for IV where the pH is almost neutral (pH = 6.0–6.6), similar to the values found in 160.01 (see Table 2 and Fig. 5A). Moreover, where available (i.e. I–IV), the pH in OS mirrors the corresponding values in SS, although the sediment colour and texture of the two layers are different, matching what found in SU-2 and SU-3 in 160.01 and in agreement with XRD analysis. Total organic carbon (TOC%) in OS (see Table 2 and Fig. 5B) ranged from 1.4 to 12.9 %, with a mean value of 6.0 ± 2.4 %. Conversely, in SS samples, the amount of TOC% (from 0.3 to 0.8 %; mean 0.66 ± 0.25 %), was significantly lower than in OS (Student t-test provided p-value = 5 × 10<sup>-4</sup>). Once more, the chemistry of OS and SS mirrors the behaviour found in SU-2 and SU-3, respectively. In addition, in OS and SS, the amount of inorganic carbon is lower than the limit of detection, indicating a scarce contribution from both authigenic and allochthonous

carbonates. Elemental analysis of the samples provided the concentration values of TE and REE reported in Table 2. Due to the large number of variables, the chemical information was summarized through principal component analysis (PCA), including samples from 160.01 for comparison.

As reported in the biplot shown in Fig. 6A, the first two components (*i.e.*, PC1 (~43 %) and PC2 (~19 %)) explain ~62 % of the total variance. The PC1 is characterized by higher negative loadings of Al (~−0.916), Sc (~−0.951), Mg (~−0.869), Ca (~−0.887), and Sr (~−0.897), which, in conjunction with the almost complete absence of carbonates, suggest that alkaline earth elements are more likely associated with clayey minerals rather than to carbonate. As shown in Fig. 5C, samples from 160.01 and IV are characterized by higher negative values of PC1, corresponding to the samples where pH is almost neutral. Interestingly, PC1 negatively correlates with pH ( $r = −0.834$ ;  $p$ -value  $<10^{-5}$ , see also Fig. 6B), indicating that more positive values of PC1 are associated with neutral pHs. Conversely, no significant correlation between PC1 and TOC% ( $r = 0.199$ ;  $p$ -value = 0.44) was found. PC2 is characterized by negative loadings of Co (~−0.915), Cu (~−0.803) and Ni (~−0.605), and positive loadings of K (0.706) and Rb (0.664). PC2 significantly correlates with TOC% ( $r = −0.822$ ;  $p$ -value =  $2 \times 10^{-4}$ , see also Fig. 6C) and does not correlate with pH ( $r = −0.186$ ;  $p$ -value = 0.47). Although slightly, PC2 separates the more organic OS (and SU-2) samples from the clayey-silt SS (and SU-3). Moreover, it is interesting to note that SS-VII is characterized by high positive values of PC1, indicating a different chemical composition compared to the other samples, consistently to what previously evidenced by XRD analysis.

It is also interesting to note that the distribution of Pb is not homogenous (see Fig. 5E). While lower concentrations of Pb were found in 160.01 and in spots I-V (20–40 mg kg<sup>−1</sup>), corresponding to the deepest part of the cave (**Section C-D** in Fig. 1), from the proximity of the lateral branch toward the entrance (Section A-C in Fig. 1), the Pb concentration was about 10–20 times higher (200–800 mg kg<sup>−1</sup>).

### 3.3. Bat guano deposit

The chemical analysis of the guano found at the mound is reported in Tables 3 and 4. The pH of the guano was approximately 3.2, in line with values reported in the literature (Audra et al., 2019; Mulec and Dietersdorfer, 2016; *i.e.* pH = 3.5). The elemental analysis showed that the bat guano is particularly enriched in K (5.7 g kg<sup>−1</sup>), Ca (5.4 g kg<sup>−1</sup>) and Mg (3.7 g kg<sup>−1</sup>) consistently with literature results (Tsalickis et al., 2021; Johnson and Vincent, 2020; Misra et al., 2019; Queffelec et al., 2018). The concentration of Pb (~2 mg kg<sup>−1</sup>) is similar to what reported by Chung et al. (2024) (2.3 mg kg<sup>−1</sup>) and Altintas et al. (2005) (2.2 mg

kg<sup>−1</sup>), although samples analysed in these studies were collected in Taiwan and Turkey (Çorum), respectively. However, lead concentrations of ~2 mg kg<sup>−1</sup> are slightly lower than what reported by Forray et al. (2024) (14.8 mg kg<sup>−1</sup>) and Amin-Rasouli et al. (2023) (5–10 mg kg<sup>−1</sup>) found in Romania and Iran. Copper concentration (740 mg kg<sup>−1</sup>) resulted in line with literature, where values between 80 and 8000 mg kg<sup>−1</sup> are generally reported (Forray et al., 2024; Johnson and Vincent, 2020; Queffelec et al., 2018; Wurster et al., 2015; Altintas et al., 2005; Miko et al., 2001). The analysis of the faecal steroids provided values consistent with those reported by Gallant et al. (2021) in insectivorous bat species, although their results demonstrate a large individual variability. However, despite the large variability, bat guano showed a larger abundance of sterols (~93 %) compared to stanols. The most abundant sterols, *i.e.* cholesterol and β-sitosterol, showed a prevalence of the former, consistently with Gallant et al. (2021).

In proximity to X, the bat guano mound (1.5 m high and 3 m wide) attested to the presence of a migratory bat colony, as previously documented by Bertini et al. (2016) and Vernier (2000). The <sup>14</sup>C age of the guano bulk (sample G1-X\*), corresponding to the centre of the mound at approximately half the total height, suggests that the guano deposit is quite recent (see Table 1), as the centre is likely not older than approximately 1950 CE. Assuming an almost constant guano deposition rate, we estimate that the accumulation rate might be about 1.5–5 cm year<sup>−1</sup>, consistent with the findings of Reid et al. (2022) and Condoinnes et al. (2002), who reported accumulation rates of 3.3 and 2.6 cm year<sup>−1</sup>, respectively, although in different contexts. A more detailed investigation of bat guano deposition processes is beyond the scope of this paper, but it is worth noting the presence of a blackish lateral band, approximately 1–1.5 m high, on the cave walls. This band is present along almost the entire wall and, based on visual and tactile inspection, the blackish colour might be attributed to bat guano input. The blackish deposit was also observed under the horizontal crests of the wall, making direct deposition unlikely. Additionally, more recent guano excretions were diffusely observed on the cave floor.

## 4. Discussion

### 4.1. The origin of the sediments

The SU-3 deposit in trench 160.01 mainly formed from allochthonous material transported by sheet-wash on the overlying limestone plateau. The transported load consisted of both eroded fragments of pre-existing soil with an argillic horizon and loess or loess-like sediments that had not yet undergone significant pedogenesis. These sediments then infiltrated the cave through the karst system. XRD analysis

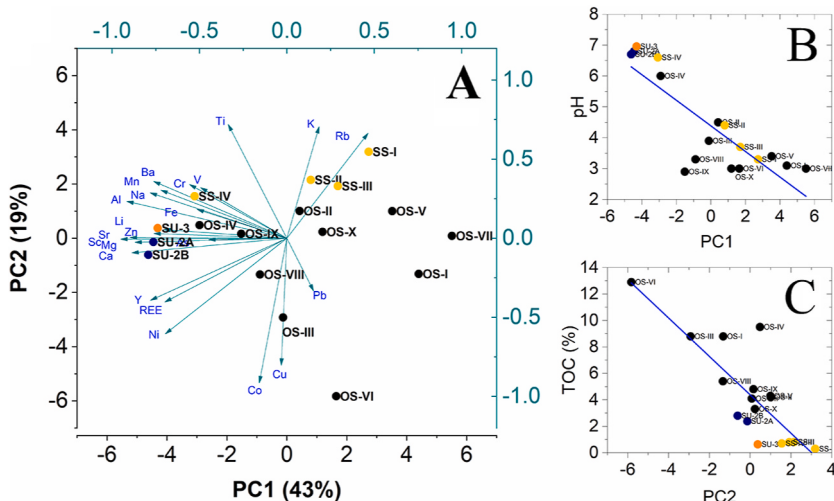


**Fig. 6.** (A) PC2 vs PC1 biplot (B) pH vs PC1 (C) TOC (%) vs PC2.

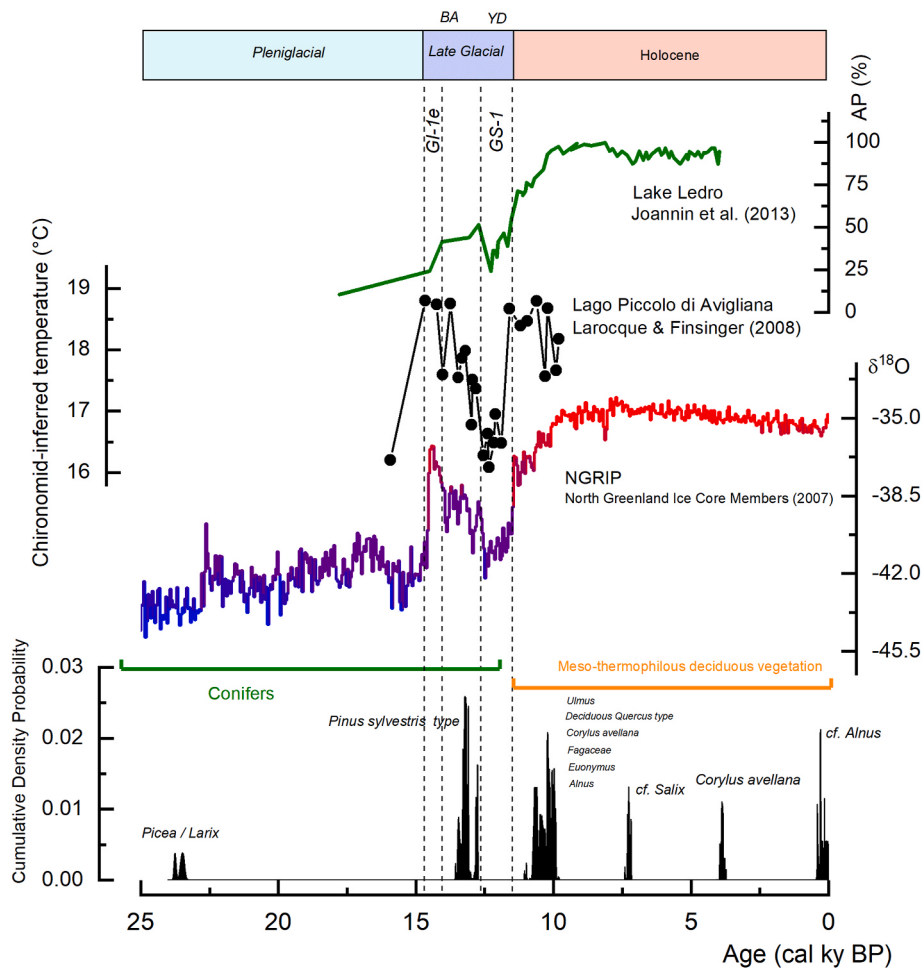


**Fig. 7.** Cumulative density probability of the  $^{14}\text{C}$  calibrated ages of charcoal vs Age. Anthracological data are indicated to the corresponding charcoal sample. In blue-red the  $\delta^{18}\text{O}$  record from (NGRIP, 2004; North Greenland Ice Core Project Members (2007); The interstadials Bølling-Allerød (BA) and the Younger Dryas (YD) are indicated. Chironomid-inferred temperature (Joannin et al., 2013) and arboreal pollen record (Larocque and Finsinger, 2008) from Lago Piccolo di Avigliana and Lake Ledro, respectively, are reported to illustrate regional scale climate.

**Table 4**  
PC1 and PC2 loadings.

| Element | Li     | Na     | K      | Rb     | Mg     | Ca     | Sr     | Ba     | Al     | Sc     | Ti     |        |
|---------|--------|--------|--------|--------|--------|--------|--------|--------|--------|--------|--------|--------|
| PC1     | -0.705 | -0.782 | 0.158  | 0.465  | -0.869 | -0.887 | -0.897 | -0.763 | -0.916 | -0.951 | -0.336 |        |
| PC2     | 0.054  | 0.287  | 0.706  | 0.664  | -0.026 | 0.093  | 0.004  | 0.360  | 0.234  | -0.006 | 0.720  |        |
| Element | V      | Cr     | Mn     | Fe     | Co     | Ni     | Cu     | Zn     | As     | Pb     | REE    | Y      |
| PC1     | -0.493 | -0.557 | -0.721 | -0.514 | -0.158 | -0.696 | -0.032 | -0.760 | -0.447 | 0.153  | -0.699 | -0.780 |
| PC2     | 0.321  | 0.340  | 0.305  | 0.183  | -0.915 | -0.605 | -0.803 | 0.030  | -0.009 | -0.334 | -0.404 | -0.392 |

confirms the presence of K-feldspar and muscovite consistent with the allochthonous origin of the sedimentary material. The presence of aeolian sediments on the Lessini plateau is well-documented in multiple physiographic contexts, such as infillings in caves and rock shelters, on alluvial terraces, and along the internal valleys of the plateau, often in association with remnants of Terra Rossa-type paleosols. At Riparo Tagliente in Valpantena, two phases of loess deposition have been documented, matching the peak of two Upper Pleistocene glacial cycles (Castiglioni et al., 1990), comparable to contemporary loess sequences in northern Italy, particularly in nearby Val Sorda (Cremaschi, 1990; Ferraro, 2002; Ferraro et al., 2004). The stratigraphic sequence at Grotta di Fumane presents a more complex scenario, with phases dominated by aeolian deposits alternating with phases dominated by thermoclastic breakdown of cave walls, accompanied by cryoturbation features (Peresani et al., 2008). The Fumane sequence begins in late Marine

Isotope Stage 5 (MIS 5), spans MIS 4 and MIS 3, and concludes at the onset of MIS 2. Whereas the lower portion is dominated by colluvial processes tied to water availability and a temperate climate, the subsequent units reflect a harsher climate, inducing thermoclastic processes on the rock-shelter walls and a marked influx of aeolian dust (loess). These alternating arid and humid phases suggest a period of high-frequency climatic instability, especially during MIS 4, correlating closely with Upper Pleistocene climatic variations recorded in the Northern Hemisphere (Cremaschi and Ferraro, 2021).

Accordingly, the original sediments of SU-3 were likely deposited on the plateau overlying the cave during the Last Glacial Maximum (LGM, MIS 2) and were later washed into the cave in the early stages of the Late Glacial (Rasmussen et al., 2014; Ravazzi et al., 2007). As climatic conditions became more humid, matrix sediments filled the interstices of the SU-4 breccia. The onset of hydromorphic conditions is

microscopically evidenced by polyconcave voids arising from ground-mass collapse due to water oversaturation, together with redox pedo-features (e.g., nodule formation and Fe-Mn impregnation of faunal remains). Horizontal clay intercalations that formed in situ are likely related to micro-runoff events that locally reworked the sediment (Williams et al., 2018). Hematite impregnation in the micromass is also notable, presumably stemming from alteration of the local outcrop along a basaltic vein.

The highly organic horizon (Ah), SU-2B, developed atop the geo-genic deposit SU-3. This paleosol, approximately 20 cm thick, contains abundant anthropogenic components (charcoal fragments, flint artifacts) and increased organic matter, as confirmed by chemical analysis. The thickness of SU-2B suggests a steady yet moderate supply of sediment of the same origin as SU-3, as indicated by XRD and chemical analyses. Lower mineral abundance in SU-2 is likely tied to dilution effects from higher organic matter inputs. Pedorelicts dispersed in the micromass are commonly rounded or subrounded, often nucleus-type, having formed around rock fragments (basalt, flint), implying a rolling action of grains. Less frequent are browned/rubefied pedorelicts in lamellar or subangular shapes, along with fragments of clay coatings (*papules sensu* Brewer, 1964). Pronounced post-depositional deformations at the contact between SU-3 and SU-2 point to a density contrast in the sediments, potentially stemming from reduced soil moisture following surface desiccation, though liquefaction-fluidization processes related to seismic activity or sudden overloading (collapse) cannot be excluded. Radiocarbon dating of charcoals from SU-2B, despite the absence of a clear chronological sequence, suggests that SU-2 formed around 13,000 cal y BP, at the end of the Bølling-Allerød interstadial. Anthropogenic input in SU-2 is highlighted by abundant millimetric charcoal fragments, microcharcoal, small organic particles, and partly combusted, decomposed plant tissues (Herbaceous Partly Burnt).

Although the cave hosts a bat colony, the near-neutral pH values and the absence of a typical faecal steroid profile linked to guano suggest that the organic matter in 160.01 derives only partially from bat guano. Instead, the observed steroids may originate from larger mammals (fauna or humans), which produce 5 $\beta$ -congeners (Bortolini et al., 2024; Bull et al., 2002) mainly detected in SU-2, or from degraded plant material containing phytosterols (e.g., campesterol,  $\beta$ -sitosterol, stigmasterol) more abundant in SU-3 (Reeves and Patton, 2005). Therefore, the higher organic matter in SU-2 compared to SU-3 could be autochthonous, resulting from local anthropogenic or faunal activity that intensified after the Bølling-Allerød interstadial; or allochthonous, carried into the cave along with clastic sediment. The warmer and more humid conditions since the Glacial-Holocene transition may have also increased the external supply of organic material, thus boosting its presence in the allochthonous load.

Although a complete stratigraphy of the cave infill is not yet available, sediment colour, texture, bulk chemistry abundance of charcoal fragments, suggest that the layer OS corresponds to unit SU-2, whereas layer SS corresponds to unit SU-3. For the sake of clarity, we hereinafter designate sediments from OS and SU-2 as OS-type, and those from SS and SU-3 as SS-type. The XRD spectra of OS-I–IV and SS-I–IV closely resemble those of SU-2 and SU-3, suggesting a broadly shared nature of the clastic fraction (see Fig. 4). The organic carbon content in the OS and SS samples also closely matches that in SU-2 and SU-3, respectively (see Fig. 5). Marked differences do emerge in sediments from OS-V–X (Figs. 4 and 5), primarily due to in situ post-depositional alterations, as detailed below.

Minor discrepancies are evident in OS-IV, where XRD analysis detected goethite. Chemical analysis also revealed significant enrichments in Fe (1.83), V (1.50), and As (3.5), likely resulting from localized input linked to the nearby ochre vein, as suggested by the chemical composition and XRD pattern of pure ochre samples (Table 2 and Fig. S1 in Supporting Material). The occurrence of goethite exclusively in OS-IV can be explained in two ways. First, it may have been introduced by

ochre extraction activities, which left considerable fragments in place. Alternatively, the relatively high pH in OS-IV (around 6.0), consistently higher than in other sediments (pH ~3–4, except for 160.01), could have inhibited iron oxide and hydroxide solubilization, reducing their mobility compared to other sediments. This explanation does not contradict the absence of goethite in 160.01, given that 160.01 is farther from the ochre vein.

OS-type sediment contains a mixture of allochthonous material, resembling SS-type, and autochthonous input mainly derived from bat guano, charcoal and basalt in the coarser mineral fraction. The relatively large size of the charcoal fragments points to an anthropogenic origin, since water percolation from overlying soils, aeolian transport, or lateral water flow within the cave (discussed later) seem less plausible transport mechanisms for charcoal. Alluvial transport from the cave mouth is also unlikely, given the increasing slope from the entrance and the configuration of the external environment. The in situ anthropogenic origin of charcoal is corroborated by a negative interface interpreted as a post-hole, where charcoals date to 12,836–12,740 cal y BP.

The source of organic matter in OS-type sediment remains partly enigmatic. As noted in SU-2, it cannot be attributed solely to bat guano. The higher sterol concentrations in OS-type relative to SS-type, combined with their greater lateral variability, may instead reflect intensified use by humans or other terrestrial mammals after the end of the Bølling-Allerød interstadial.

#### 4.2. In situ chemical alterations

The in situ chemical alteration of the sediment primarily stems from the uneven deposition of bat guano, which affects sediment pH. With the exception of 160.01 and Spot IV, all other samples show markedly low pH values (3–4.5), consistent with incomplete neutralization of acidic compounds generated by bat guano degradation (Audra et al., 2021; Wurster et al., 2015; Onac, 2012). Although fresh bat guano is generally neutral or slightly alkaline (Ferreira et al., 2007), its microbial decomposition produces phosphoric, sulfuric, and nitric acids, which can lower the pH to between 2 and 4 (Audra et al., 2019; Miko et al., 2002). In humid conditions, these acids diffuse downward through vertical percolation (Audra et al., 2019), explaining why no significant pH differences are observed between the OS-type and the underlying SS-type.

In 160.01 and Spot IV, higher pH values likely reflect limited guano input, as the lower height of the vault may have restricted bat access. This explanation is supported by the absence of carbonates in these sediments, alongside trace amounts of guano-derived minerals, indicating that bat guano input in these areas was never extensive. The moderate acidity produced by guano breakdown, likely arising in the uppermost layers (i.e., SU-2 or OS-IV) and percolating downward, promoted bone dissolution in SU-3. However, this mild acidity was quickly neutralized by carbonate minerals; as the carbonates dissolve, the pH returns to near-neutral levels.

In other areas, especially along section B–C (Fig. 1), the pH is more acidic. A decline in pH intensifies post-depositional sediment alteration. Principal Component Analysis (PCA) reveals that the chemical characteristics of the sediments can be effectively captured by the first two principal components (PCs), which together account for 62 % of the total variance. The influence of pH-induced alteration can be isolated from the natural variability of OS-type and SS-type sediment by examining PC1, which shows a strong correlation with pH (Fig. 6). In contrast, PC2 appears to reflect the inherent chemical differences between OS-type and SS-type matrices. As shown in Fig. 6, PC1 is characterized by higher negative loadings of alkaline earth elements (Ca, Mg, Sr) as well as Al and Sc. The lower concentrations of alkaline earths, under acidic conditions, may result from increased solubility and subsequent leaching. At the same time, more acidic conditions typically coincide with higher guano input, causing structural changes in the sediment. This is evident from XRD analyses showing the formation of taranakite, a mineral stable in acidic environments that precipitates

where guano contacts clay under poor drainage (Onac, 2012). Tarakite was unambiguously identified only in section B-C, which is more acidic than section C-D (see Fig. 5-A).

Moreover, a relatively drier environment is inferred in section C-D, based on micromorphological evidence (spore colonies) suggesting prolonged soil exposure of SU-2 in 160.01. By contrast, lead concentrations (Fig. 5-E) point to more sustained moisture in section B-C. Along section C-D, Pb averages  $28 \pm 4 \text{ mg kg}^{-1}$ , whereas it increases by about an order of magnitude in section B-C ( $500 \pm 250 \text{ mg kg}^{-1}$ ). The increase in Pb cannot be attributed to bat guano ( $\sim 2 \text{ mg kg}^{-1}$ ) and likely reflects more recent anthropogenic activities outside the cave (Pasquetti et al., 2025). Although recent in origin, the high lead content in section B-C traces the main water flow pathway from the east, bypassing section C-D. The combination of greater acidity and higher moisture in section B-C is probably responsible for the higher tarakite formation in these sediments.

#### 4.3. Deposition dynamics

Based on the morphological and physicochemical characteristics of the sediments, we tentatively propose the following depositional model. Prior to the Bølling-Allerød interstadial, the sediment load was predominantly allochthonous, consisting of loess-like deposits that were low in organic matter and contained only minor autochthonous contributions (i.e., SS-type deposits). This material was likely introduced via slow percolation from the plateau, resulting in a low-energy depositional environment. The absence of charcoal fragments suggests a limited or negligible human presence, whereas evidence for faunal use is scarce due to the degradation of bone remains.

In principle, SS-type deposits would be expected throughout the cave. However, from the intersection with the lateral branch (C in Fig. 1) to the cave entrance (A), this type of sediment was not found. We hypothesize that much of the original SS-type deposit was removed by hydrological erosion events at the end of the Glacial. The presence of a carbonate concretion at the lateral branch's terminus (E in Fig. 1) and the Pb concentration pattern (Fig. 5E) both support this interpretation. The flow of supersaturated water over the carbonate testifies to predominant hydrological activity in the lateral branch (E), with water following the pathway E-C-B-A and only marginally affecting section C-D. This hydrological activity may have intensified during the post-Glacial warming, leading to substantial removal of SS-type sediment from much of the cave.

From the Bølling-Allerød interstadial into the Holocene, human use of the cave increased significantly, as indicated by the abundance of charcoal fragments in OS-type sediments relative to SS-type. Although dating of the guano mound indicates it formed within the last century, earlier bat occupation cannot be excluded. The current migratory behaviour of the bat colony aligns with increased bat activity following the onset of a more temperate climate. The acidic sediment conditions, presence of guano-derived minerals, and a roughly 1-m-wide blackish lateral band on the cave walls suggest that guano deposition may have been more extensive in the past than it is today. While an exact timeline is not yet clear, it appears plausible that humans and bats coexisted during the Holocene, generating autochthonous inputs of charcoal, organic matter, and guano that collectively formed the OS-type sediment.

The absence of an extensive guano deposit - apart from the recent mound - can plausibly be attributed to past small-scale extraction for agricultural use. Although such practices are not documented in this region, large-scale guano mining has been recorded in South America since the 19th century, spurred by the global expansion of agriculture (Haller, 2022; Cushman, 2017). According to the cave owner, Mr. Bruno Lavarini, a local farmer (Pietro "Tiglio"), removed much of the cave's organic infill between 1955 and 1965 CE, carrying it out with a traditional basket (*gerla* or *zerlo*) to fertilize a field that once occupied the area of the present-day car park above the site. Mr Lavarini's account fits

closely with the radiocarbon age of the guano mound as well as with the occurrence of the dark organic band preserved in the cave wall. Such guano harvesting could also explain the scarcity of charcoal fragments younger than  $\sim 10,000 \text{ cal yr BP}$ , which may have been removed along with the guano. Alternatively, the reduced cave use during the Mid-to-Late Holocene seems less likely given the abundant archaeological evidence for human activity in the wider region (Mussi and Peresani, 2011; Bortolini et al., 2021).

#### 4.4. Prehistoric frequentation of the cave

Veja cave A locates in the Monti Lessini, which are part of the Veneto-Friuli Pre-Alps, a  $\sim 40 \text{ km}$ -wide, where peaks top over 2000 m and 1000–1200 m karst plateaux are carved by gorges, river valleys and alpine lakes. Soon after Last Glacial Maximum (LGM), glaciers retreat from the Pre-Alpine piedmont and the Great Adriatic-Po Plain was submerged (Peresani et al., 2021), the Epigravettian hunter-gatherers began to occupy the Pre-Alps during the Late-Glacial (Ravazzi et al., 2007; Angelucci and Bassetti, 2009).

During the Late Würm period, associated with the LGM, the presence of conifers in the arboreal vegetation, *Picea* and/or *Larix*, documented between 23,800 and 23,300 cal y BP (Fig. 7), is plausible in Veja, similar to the submontane belt of the Veneto and Friuli plains (Pini et al., 2009, 2010). Their presence was reduced and restricted to limited ecological conditions compared to previous interstadial phases. The cold and dry climate of the most extreme glacial conditions in Late Würm favoured in fact the development of steppe and xerophytic scrub ecosystems dominated by *Pinus sylvestris/mugo* pollen (Pini et al., 2009, 2010).

Climatic conditions profoundly changed at the onset of Greenland Interstadial 1 (GI-1), the Late-Glacial interstadial, triggering widespread deglaciation and promoting general geomorphological stability across much of the Southern Alps up to mid elevations. The warming of the Bølling period (GI-1e) activated a large-scale vegetational shift even at regional scale (Joannin et al., 2013; Larocque and Finsinger, 2008), consisting in the expansion of forests and the rapid uplifting of the treeline by  $\sim 800$ – $1000 \text{ m}$  to over  $1500 \text{ m a.s.l.}$  at the end of the Bølling-Allerød interstadial (Friedrich et al., 2024; Vescovi et al., 2007). In Veja, the presence of conifers of *P. sylvestris* type is confirmed by radiocarbon dating, which dates the anthracological samples between 13,600 and 12,800 cal y BP (Fig. 7). This evidence is consistent with exalpic submontane palynological sequences, which attest to the prominent role of *P. sylvestris* in local forest formations during the Bølling-Allerød interstadial, originally co-associated with *Betula*, *Picea*, *Larix*, and after 13,500 cal y BP with thermophilic broadleaves (Finsinger et al., 2011; Ravazzi et al., 2007).

The interstadial GI-1 was followed by the Younger Dryas (YD) cooling (GS-1), a climatic oscillation marked by a sharp, decades-long drop in temperature, accompanied by drier conditions and negative winter precipitation anomalies (Baroni et al., 2021; Ivy-Ochs et al., 2009). The consequences for the biological communities included a synchronous, rapid vegetation contraction, an about 200–300 m shift in treeline altitude, and the expansion of grassland and steppe environments. Nevertheless, pollen records from Palughetto (Cansiglio Plateau) and Pian di Gembro (Valtellina) reveal that the treeline was still lowering above 1400 m (Friedrich et al., 2024; Vescovi et al., 2007).

Finally, climatic warming and increased rainfall at the onset of the Holocene (11,700–11,500 cal yr BP) fostered the rapid expansion of thermophilous trees (Vescovi et al., 2007). In this phase, 8 charcoal samples (out of 19 sent for radiocarbon dating) fall within a time range between 11,000 and 9000 cal yr BP (Fig. 7). The anthracological record refers to deciduous broadleaved trees, such as *Alnus*, *C. avellana*, *Ulmus*, and deciduous *Quercus*, characteristics of meso-thermophilous communities. In detail, the data collected are similar to the anthracological analyses carried out on a larger sediment sample (SU-2A; Ghezzo et al. in preparation). In this context, the Holocene level revealed charcoal from tree taxa typical of moist and nutrient-rich soils. The SU-2A dataset

combines pioneer or permanent forest habitats, including light-demanding (such as *Q. petraea/robur* and *F. angustifolia/exelsior*) and shade-tolerant (*F. sylvatica*) trees. Since the Early Holocene, mesophilous coenosis appear to have characterised the Venetian exalpic submontane belt.

Late Epigravettian hunter-gatherers inhabited this mountain region since 14,000 cal yr BP, as testified by over 50 sites surveyed, mapped and explored during the last six decades, starting soon after the first pioneering excavation conducted in 1964 at the mountain site of Riparo Battaglia on the Sette Comuni Plateau. Camps distribute at different elevations in valley bottoms up to the middle mountain range, mostly in the vicinity of peat bogs or landmarks, as single or multiple occupation sites (Broglio, 1993; Bertola et al., 2007; Mussi and Peresani, 2011). Archaeological records reveal that subsistence was mostly based on hunting of ungulates like red deer, ibex, chamois, roe deer, alongside with some carnivores, as well as on specialized hunting of marmots (Nannini et al., 2022; Duches et al., 2014; Tagliacozzo and Fiore, 2009).

Since the first discoveries, countless of studies contributed to reconstruct the Epigravettian colonization of the Alps (see Montoya et al., 2018 for references) and to relate it to the major environmental shifts (Manzella et al., 2024). Several of these works analyse the distribution of radiocarbon dates and other proxies for human frequentation rates (Naudinot et al., 2014; Schmidt et al., 2025). Particularly, Naudinot et al. (2014) considered 45 dates obtained since the early 1970s by different facilities and examined their cumulative probability-density distribution, which showed a clear increase between 14,200 and 13,500 cal BP. Before that interval, a sparse set of dates from only one site, Riparo Tagliente, is the only available record testifying the earliest human presence at the Alpine slope foot soon after the end of the LGM (Bortolini et al., 2021; Fontana et al., 2018). The peak in the summed-probability curve and the inferred population increase at the beginning of the Bølling-Allerød warming were interpreted as an expression of the recolonization model - an occupation strategy in which Epigravettian groups moved into mountain environments after the disappearance of a large part of the Great Adriatic Po Plain (Peresani et al., 2021; Ruiz-Redondo et al., 2022). This peak has also been observed in Veja cave A and further indicates that the Late Epigravettian penetration was firstly limited to valleys and plateaus around 500 m asl, reaching mid-altitude territories during the second part of the Late Glacial interstadial. Since the earliest exploitation of hunting basins 14,000 cal yr BP, it was during the Allerød that the mountain ecotone was reclaimed by Epigravettian hunters addressed to ungulates and marmots. A logistical occupation network based on seasonal mobility patterns and functionally complementary sites was developed by these foragers well-adapted to exploit the range of biological resources (Romandini et al., 2012; Fontana et al., 2018b; Nannini et al., 2022).

As shown in Fig. 7, after the Bølling-Allerød interstadial phase, the distribution of dates marks a critical gap in coincidence of the YD. However, the hiatus observed in Veja cave resulted narrower than in Tuscany and Liguria-Provence arc, the two other regions where this proxy has been investigated (Naudinot et al., 2014). Although GS-1 strongly affected regional biomes, its impact on hunting territories and settlement patterns appears limited, as human activity is still attested by anthropogenic signature in the same areas occupied during the GI-1 interstadial. Epigravettian camps are mostly open-air sites located close to lakes or wetlands, well above 1000 m of altitude, framed in the seasonal frequentation of the inner Alps and Dolomitic zone up to 1500 m asl. Compared to the previous phase, camps are smaller, fewer, and contain simpler lithic assemblages with less complex spatial organization (Mussi and Peresani, 2011; Cattabriga and Peresani, 2024). The trend toward increasing simplification of settlement, contraction of flint scatters and reduction in anthropogenic indicators, suggests briefer occupation and greater mobility pattern (Mussi and Peresani, 2011; Duches et al., 2014). Culturally, the YD coincides with the appearance of trapezoids, a lithic element possibly used in hunting practises, which remains quite unknown elsewhere in Italy and marks a distinctive

chrono-cultural horizon in the recent Epigravettian (Dalmeri et al., 2004; Fasser et al., 2024).

The collapse of radiocarbon dates at the YD-Holocene transition coincides with the terminal Epigravettian, a chrono-cultural phase poorly dated despite the presence of well-studied sites. This gap has been attributed to sampling bias (Naudinot et al., 2014), and effect partly reduced by new dates from Riparo Cornafessa, a mid-elevation shelter in the high Monti Lessini, that was settled during the YD. These dates reinforce the evidence for human presence in the highlands. Further downslope, at the south-western edge of Monti Lessini on the left bank of the Adige River, archaeological layers of Phase II at Riparo Soman have yielded a fireplace, backed points, microliths, common tools, and bone remains of adult chamois and ibex, followed by red deer and bovids, resulting from summer- and autumn-season hunting (Tagliacozzo and Cassoli, 1994).

We cannot rule out the possibility that the frequency hiatus of dates during the YD at Veja A cave is only apparent. In fact, summed-probability distributions can display artificial gaps, especially immediately before the YD, at its onset and at the boundary with the Preboreal, as observed by Bamforth and Grund (2012). Discontinuities in the archaeological record can lie in factors such as erosion, lack of diagnostic artifacts, changes in settlement strategies, and the complexity of the evolution of human settlement patterns. No site does not mean no human. Rather, the ways in which people used the territory reflects on the archaeological visibility, site distribution in the landscape and site density. Nevertheless, any assessment of the radiocarbon gap must account for the modes and goals of occupation at Veja. A hypothetical hiatus in YD use would most plausibly signal a contraction of the tasks that had previously motivated Epigravettian groups to enter the cave. Several contextual clues point in this direction, such as large charcoal chunks and a post-hole at the terminus of the main branch of the cave coincide with the ochre vein exposed in branch C-D (Fig. 1).

Taken together, these data suggest that the cave had been visited during GI-1 and a renewed exploitation occurred in the Holocene, possibly to extract this mineral. Broad-scale ochre use for utilitarian, symbolic and artistic purposes is well attested across Monti Lessini (see Cavallo et al., 2018, among the others). The pronounced climatic instability characterising the YD may have curtailed social complexity, fostered greater residential mobility, and simultaneously dampened the interest in extracting ochre.

However, a cautious interpretation of the summed-probability curves for the Pleistocene-Holocene boundary at Veja cave A must account for the possibility of high residential mobility and for land-use strategies focused on short-terms logistical activities conducted from small, archaeologically inconspicuous camps. An increase in the frequency of residential moves would reduce both site density and the number of datable contexts detectable by archaeologists.

## 5. Conclusion

This study examines the sedimentary infill of Cave A at Ponte di Veja (Verona, Italy) to reconstruct its provenance, post-depositional alteration, and depositional history. The lowermost unit here investigated, SU-3, is interpreted as an allochthonous loess- and soil-derived deposit formed at the Last Glacial Maximum by slow percolation from the overlying karst plateau. Overlying SU-2B (OS-type paleosol, ~20 cm) formed ~13,000 cal yr BP. Charcoal and organics indicate local human activity, large-mammal inputs, and bat guano. OS and SS layers share the same external clastic source but diverged slightly through post-depositional changes. Microbial guano breakdown generates strong acids that keep most sediments acidic (pH ≈ 3–4.5), whereas trench 160.01 remains near-neutral where guano input is limited and carbonate buffering is effective. Principal-component analysis links higher acidity to leaching of alkaline-earth elements and to precipitation of taranakite, concentrated in the wetter, more acidic sector of the cave (i.e. B-C).

These data support a four-stage model: (1) pre-Bølling-Allerød

infilling by loess-rich SS-type sediment delivered by infiltration; (2) post-glacial runoff removing much of this deposit; (3) Bølling–Allerød and Holocene re-occupation by humans and bats, with charcoal-rich OS layers and guano deposition (4) substantial removal of guano, with younger charcoal, by a local farmer in 1955–1965 CE, matching radiocarbon ages of the residual mound and explaining scarce mid-to late-Holocene traces.

The sequence mirrors Late-Glacial climate. At the onset of the Late-Glacial interstadial the number of dated sites rises sharply, reflecting intensified Epigravettian use of the Pre-Alps. Harsher Younger Dryas conditions prompted smaller, task-specific logistical camps, simpler lithic assemblages and higher residential mobility, all of which reduce the density of datable anthracological evidence complements this picture. Of eighteen analysed fragments eleven derive from deciduous taxa typical of modern local woodland, while seven belong to *P. sylvestris* conifers. Exclusively coniferous charcoal before the end of the Bølling–Allerød aligns with GI-1 environmental conditions, whereas Early-Holocene samples capture the spread of thermophilous forests. Overall, Cave A provides a coherent geoarchaeological record linking climate change, bat colonization, and Epigravettian land use in the Southern Pre-Alps.

#### CRediT authorship contribution statement

Dario Battistel: Writing – review & editing, Writing – original draft, Methodology, Investigation Formal analysis, Data curation, Conceptualization. Mara Bortolini Methodology, Investigation Formal analysis, Data curation. Anna De Rossi, Investigation, Formal analysis. Michele Bassetti: Methodology, Investigation Formal analysis, Pietro Riello: Writing – review & editing Investigation Formal analysis, Data curation, Conceptualization. Marta Radaelli: Investigation, Formal analysis. Andrea Pereswiet-Soltan: Investigation and Conceptualization. Leonardo Latella: Writing – review & editing, Conceptualization. Mauro Buonincontri: Methodology, Investigation, Formal analysis, Writing – review & editing. Francesco Sauro: Investigation, Conceptualization. Paola Salzani: Investigation, Conceptualization. Elisabetta Cilli: Investigation, Conceptualization. Marco Peresani: Writing – review & editing, Writing – original draft, Conceptualization. Elena Ghezzo: Supervision, Funding acquisition, Writing – review & editing, Conceptualization.

#### Declaration of competing interest

The authors declare that they have no known competing financial interests or personal relationships that could have appeared to influence the work reported in this paper.

#### Acknowledgements

This research was conducted in the framework of the REFIND Project (Remote strategies for fossil finding– This project has received funding from the European Union's Horizon 2020 research and innovation programme under the Marie Skłodowska-Curie grant agreement No.785821 (MSCA-IF-GF).

#### Appendix A. Supplementary data

Supplementary data to this article can be found online at <https://doi.org/10.1016/j.quascirev.2025.109619>.

#### Data availability

All data and/or code is contained within the submission.

#### References

- Abbate Edlmann, M.L., Luca, L. de, Lazzeri, S., 1994. Atlante Anatomico Degli Alberi Ed Arbusti Della Macchia Mediterranea. Istituto Agronomico per l'Oltremare, Florence.
- Altıntaş, A., Kontaş, T., Yıldız, G., Erkal, N., 2005. Yarasa dışkısı (bat guano) mineral düzeyleri. Ankara Univ. Vet. Fak. Derg. 52 (1), 1–5.
- Amin-Rasouli, H., Minami, M., Armstrong-Altrin, J.S., Jou, N.H., Moradi, M., 2023. Geochemistry and <sup>14</sup>C dating of guano deposits in the Karafut Cave, Kurdistan, Iran: implication for paleoenvironment. Environ. Monit. Assess. 195, 1144. <https://doi.org/10.1007/s10661-023-11624-9>.
- Angelucci, D.E., 2017. Lithic artefacts. In: Nicosia, C.G., Stoops, G. (Eds.), 2017, Archaeological Soil and Sediment Micromorphology. Wiley Blackwell, Chichester, pp. 223–229.
- Angelucci, D.E., Bassetti, M., 2009. Humans and their landscape from the alpine last glacial maximum to the middle holocene in trentino: georearcheological considerations. Preist. Alp. 44, 59–78.
- Audra, P., de Waele, J., Bentaleb, I., Chroňáková, A., Krištufek, V., et al., 2019. Guano related phosphate-rich minerals in European caves. Int. J. Speleol. 48 (1), 75–105.
- Audra, P., Heresanu, V., Barriquand, L., El Kadiri Boutchich, M., Jaillet, S., et al., 2021. Bat guano minerals and mineralization processes in Chameau Cave, Eastern Morocco. Int. J. Speleol. 50 (1), 91–109. <https://doi.org/10.5038/1827-806X.50.1.2374>, 2021.
- Baker, A., Mariethoz, G., Comas-Bru, L., Hartmann, A., Frisia, S., Borsato, A., Treble, P. C., Asrat, A., 2021. The properties of annually laminated stalagmites – a global synthesis. Rev. Geophys. 59. <https://doi.org/10.1029/2020RG000722>.
- Bamforth, D.B., Grund, B., 2012. Radiocarbon calibration curves, summed probability distributions, and early Paleoindian population trends in North America. J. Archaeol. Sci. 39 (6), 1768–1774.
- Baroni, C., Gennaro, S., Salvatore, M.C., Ivy-Ochs, S., Christl, M., Cerrato, R., Orombelli, G., 2021. Last Lateglacial glacier advance in the Gran Paradiso Group reveals relatively drier climatic conditions established in the Western Alps since at least the Younger Dryas. Quat. Sci. Rev. 255, 106815. <https://doi.org/10.1016/j.quascirev.2021.106815>.
- Bartolomei, G., Broglio, A., 1975. Risultati preliminari delle nuove ricerche nei depositi quaternari della Grotta A di Veja. Bollettino Museo Civico Storia Naturale di Verona 2, 217–238.
- Battistel, D., Piazza, R., Argiradis, A., Marchiori, E., Radaelli, M., Barbante, C., 2015. GC-MS method for determining faecal sterols as biomarkers of human and pastoral animal presence in freshwater sediments. Anal. Bioanal. Chem. 407, 8505–8514. <https://doi.org/10.1007/s00216-015-8998-2>.
- Bella, P., Gradiński, M., Hercman, H., Leszczyński, S., Nemec, W., 2021. Sedimentary anatomy and hydrological record of relic fluvial deposits in a karst cave conduit. Sedimentology 68, 425–448. <https://doi.org/10.1111/sed.12785>.
- Bertini, M., Avesani, D., Latella, L., 2016. Distribuzione della fauna all'interno della Grotta A del Ponte di Veja. Quaderno Culturale - La Lessinia ieri oggi domani 57–62.
- Bertola, S., Broglio, A., Cassoli, P.F., Cilli, C., Cusinato, A., Dalmeri, G., De Stefanis, M., Fiore, I., Fontana, F., Giacobini, G., Guerrreschi, A., Gurioli, F., Lemorini, C., Liagre, J., Malerba, G., Montoya, C., Peresani, M., Rocci, R., Rossetti, P., Tagliacozzo, A., Ziggotti, S., 2007. In: Martini, F. (Ed.), L'Epigravettiano recente nell'area prealpina e alpina orientale, vol. 5, pp. 39–94 a cura di). L'Italia tra 15.000 e 10.000 anni fa. Cosmopolitismo e regionalità nel Tardoglaciale, Millenni, Studi di Archeologia Preistorica, Museo Fiorentino di Preistoria "Paolo Graziosi", Firenze.
- Biagioli, F., Coleine, C., Piano, E., Nicolosi, G., Poli, A., Prigione, V., Zanellati, A., Varese, C., Isaia, M., Selbmann, L., 2023. Microbial diversity and proxy species for human impact in Italian karst caves. Sci. Rep. 13, 689. <https://doi.org/10.1038/s41598-022-26511-5>.
- Bortolini, E., Pagani, L., Oxilia, G., Posth, C., Fontana, F., Badino, F., Saupe, T., Montinaro, F., Margaritora, D., Romandini, M., Lugli, F., Papini, A., Boggiani, M., Perrini, N., Oxilia, A., Aiese, Cigliono R., Barcelona, R., Visentin, D., Fasser, N., Arrighi, S., Figus, C., Marciani, G., Silvestrini, S., Bernardini, F., Menghi Sartorio, J. C., Fiorenza, L., Moggi, Cecchi J., Tuniz, C., Kivisild, T., Gianfrancesco, F., Peresani, M., Scheib, C.L., Talamo, S., D'Esposito, M., Benazzi, S., 2021. Early Alpine occupation backdates westward human migration in Late Glacial Europe. Curr. Biol. 31/11, 2484–2493.e7. <https://doi.org/10.1016/j.cub.2021.03.078>.
- Bortolini, M., Nicosia, C., Argiradis, E., Pojana, G., Devos, Y., Battistel, D., 2024. Fecal biomarkers in Italian anthropogenic soil horizon and deposits from Middle Ages and bronze age. Quat. Sci. Rev. 329, 108541. <https://doi.org/10.1016/j.quascirev.2024.108541>.
- Brewer, R., 1964. Fabric and Mineral Analysis of Soils. John Wiley & Sons, New York.
- Broglio, A., 1993. Mountain sites in the context of the north-east Italian upper palaeolithic and mesolithic. Preistoria Alp. 28, 293–310.
- Broglio, A., Laplace, G., Zorzi, F., 1963. I depositi quaternari del Ponte di Veja. Le industrie. Memore Museo Civico Storia Naturale di Verona 11, 325–367.
- Bronk Ramsey, C., 2021. OxCal v.4.4.4 [software]. URL: <https://c14.arch.ox.ac.uk/oxcal.html>.
- Bull, I.D., Lockheart, M.J., Elhmmali, M.M., Roberts, D.J., Evershed, R.P., 2002. The origin of faeces by means of biomarker detection. Environ. Int. 27, 647–654. [https://doi.org/10.1016/S0160-4120\(01\)00124-6](https://doi.org/10.1016/S0160-4120(01)00124-6).
- Castiglioni, G.B., Cremašchi, M., Guerrreschi, A., Meneghel, M., Sauro, U., Van Vliet, Lanoe B., 1990. The loess deposits in the Lessini plateau, in the loess in northern and Central Italy: a loess basin between the Alps and the mediterranean region, Bologna. Quad. Geodinamica Alpina e Quaternaria 1, 41–59.
- Cattabriga, G., Peresani, M., 2024. Criteria for identifying knapping skill level through the analysis of lithic cores: an example from Val Lastari, Late Paleolithic, Italy. Lithic Technol. 16. <https://doi.org/10.1080/01977261.2024.2303230>.

- Cavallo, G., Fontana, F., Gialanella, S., Gonzato, F., Riccardi, M.P., Zorzin, R., Peresani, M., 2018. Heat treatment of mineral pigment during the upper Palaeolithic in North-East Italy. *Archaeometry* 60 (5), 1045–1061.
- Cavallo, G., Ischia, G., Zorzin, R., Gialanella, S., 2021. Experimental analysis on natural heated goethite from ponte di Veja (Mt Lessini, NE Italy). *J. Archaeol. Sci.: Report* 36, 102871. <https://doi.org/10.1016/j.jasrep.2021.102871>. ISSN 2352-409X.
- Chelidonio, G., 1992. Significati della ricorrenza di industrie litiche del Paleolitico medio e superiore in Lessinia. In: *Annuario Storico Della Valpolicella*, pp. 77–82.
- Chung, K.-T., Lin, C.-L., Chuang, W.-C., Lee, M.-C., Chen, L.-W., Wu, C.-H., 2024. Pharmaceutical screening of bat Feces and their applications and risks in traditional Chinese medicine. *Separations* 11, 76. <https://doi.org/10.3390/separations11030076>.
- Condomines, M., Bentaleb, I., Filaiti, E., Robert, A., Milhas, C., 2022. Comparison of <sup>14</sup>C and <sup>210</sup>Pb - <sup>137</sup>Cs - <sup>241</sup>Am dating methods of a recent bat guano deposit (Lot, SW France). *Quat. Geochronol.* 73, 101400. <https://doi.org/10.1016/j.quageo.2022.101400>. ISSN 1871-1014.
- Cremaschi, M. (Ed.), 1990. The Loess in Northern and Central Italy: A Loess Basin between the Alps and the Mediterranean Region, Bologna, vol. 1. Quad. Geodinamica Alpina e Quaternaria, p. 187.
- Cremaschi, M., Ferraro, F., 2021. 56 TH SCIENTIFIC CONFERENCE Sciences of Prehistory and Protohistory: Palaeoecology, Archaeobiology, Digital Applications and Archaeometry FERRARA, 20-23 OCTOBER 2021. ISTITUTO ITALIANO DI PREISTORIA E PROTOSTORIA, LVI RIUNIONE SCIENTIFICA ABSTRACT BOOK, p. 4.
- Cushman, G., 2017. Guano, Intensive Agriculture, and Environmental Change in Latin America and the Caribbean. Oxford Research Encyclopedia of Latin American History from. <https://oxfordre.com/latinamericanhistory/view/10.1093/acrefore/9780199366439.001.0001/acrefore9780199366439-e-113>.
- Dalmeri, G., Ferrari, S., Peresani, M., 2004. Rise and fall in the utilization of trapezoidal microliths during the late Upper Palaeolithic in Europe - an overview from the Italian record. In: Terberger, T., Eriksen, B.V. (Eds.), Hunters in a Changing World. Environment and Archaeology of the Pleistocene-Holocene Transition (Ca. 11000 – 9000 B.C.) in Northern Central Europe. Verlag, Rahden, pp. 243–251.
- Deldicque, D., Pozzi, J.-P., Perrenoud, C., Falguères, C., Mahieux, G., Lartigot-Campin, A.-S., Rouzaud, J.-N., 2022. Traces of fire in a 560,000-year-old occupation soil at Caune de l'Arago: response to the article by Professor Henry de Lumley. *C. R. Geosci.* 354, 47–50. <https://doi.org/10.5802/crgeo.114>. <https://comptes-rendus.academie-sciences.fr/geoscience/articles/10.5802/crgeo.114/>.
- Duan, W., Kotlia, B.S., Tan, M., 2013. Mineral composition and structure of the stalagmite laminas from Chulusasim cave, Indian Himalaya, and the significance for paleoclimatic reconstruction. *Quat. Int.* 298, 93–97. <https://doi.org/10.1016/j.quat.2013.02.001>.
- Duches, R., Avanzini, M., Bassetti, M., Flor, E., Neri, S., Dalmeri, G., 2014. Évolution de la mobilité épigravettienne durant le Dryas récent: quelles nouvelles informations pour l'Italie nord-orientale. In: Langlais, M., Naudinot, N., Peresani, M. (Eds.), Les groupes culturels de la transition Pléistocène-Holocène entre Atlantique et Adriatique. Séance de la Société Préhistorique Française, vol. 3, pp. 185–203.
- Fabbris, S., Sauro, F., Santagata, T., Rossi, G., de Waele, J., 2017. High-resolution 3-D mapping using terrestrial laser scanning as a tool for geomorphological and speleogenetical studies in caves: an example from the Lessini mountains (North Italy). *Geomorphology* 280, 16–29. <https://doi.org/10.1016/j.geomorph.2016.12.001>.
- Falgueres, C., Grupponi, G., Bahain, J.J., Dolo, J.M., Peresani, M., 2025. Dating the middle palaeolithic of Fumane cave by the combined ESR/U-series method. *J. Quat. Sci.* 40, 862–875.
- FAO, 2006. Guidelines for Soil Description, fourth ed. FAO, Food and Agriculture Organization of the United Nations, Rome, p. 97.
- FAO, 2021. Standard Operating Procedure for Soil pH Determination. Rome.
- Farrand, W.R., 2001. Sediments and stratigraphy in Rockshelters and caves: a personal perspective on principles and Pragmatics. *Geoarchaeology* 16 (5), 537–557.
- Fasser, N., Visentini, D., Duches, R., Peresani, M., Fontana, F., 2024. Lithic projectile technology in the western Late Epigravettian: the case study of north-eastern Italy. *Quat. Int.* 694/10, 70–90.
- Ferraro, F., 2002. I riempimenti sedimentari delle cavità carsiche e dei ripari sottoroccia come memoria storica delle variazioni climatiche e paleoambientali del tardo Pleistocene. Unpublished PhD thesis Università degli Studi di Milano.
- Ferraro, F., Terhorst, B., Ottner, F., Cremaschi Val Sorda, M., 2004. An upper pleistocene loess-palaeosol sequence in northeastern Italy. *Rev. Mex. Ciencias Geol.* 24/1, 30–47.
- Ferreira, R.L., Proux, X., Martins, R.P., 2007. Structure of bat guano communities in a dry Brazilian cave. *Trop. Zool.* 20, 55–74.
- Finsinger, W., Lane, C.S., Van Den Brand, G.J., Wagner-Cremer, F., Blockley, S.P.E., Lotter, A.F., 2011. The last glacial *Quercus* expansion in the southern European Alps: rapid vegetation response to a late Allerød climate warming? *J. Quat. Sci.* 26, 694–702. <https://doi.org/10.1002/jqs.1493>.
- Fiore, S., Laviano, R., 1991. Brushite, hydroxyapatite, and taranakite from Apulian caves (southern Italy): new mineralogical data. *Am. Mineral.* 76 (9–10), 1722–1727.
- Fontana, F., Falceri, L., Gajardo, A., Bertola, S., Cavulli, F., Guerreschi, A., Visentin, D., 2018a. Re-colonising the southern alpine fringe: diachronic data on the use of sheltered space in the late Epigravettian site of Riparo Tagliente. In: Borgia, V., Cristiani, E. (Eds.), Palaeolithic Italy Advanced Studies on Early Human Adaptation in the Apennine Peninsula). Sidestone Press, 2018.
- Fontana, F., Falceri, L., Gajardo, A., Bertola, S., Cremona, M.G., Cavulli, F., Guerreschi, A., Visentin, D., 2018b. Diachronic data on the use of sheltered space in the late epigravettian site of Riparo Tagliente (verona, Italy). In: Borgia, V., Cristiani, E. (Eds.), Palaeolithic Italy: Advanced Studies on Early Human Adaptations in the Apennine Peninsula. Sidestone Press, Leiden, pp. 287–310.
- Forray, F.L., Dumitru, O.A., Atlas, Z.D., Onac, B.P., 2024. Past anthropogenic impacts revealed by trace elements in cave guano. *Chemosphere* 360, 142447.
- Friedrich, M., Kromer, B., Peresani, M., 2024. Late glacial tree-ring chronologies from Palughetto bog, Veneto pre-Alps, Italy. Alpine and Mediterranean Quaternary 37 (1), 53–65. <https://doi.org/10.26382/AMQ.2024.03>.
- Frost, R.L., Xi, Yunfei, Palmer, Sara J., Pogson, Ross E., 2011. Vibrational spectroscopic analysis of taranakite ( $K(NH_4)Al_3(PO_4)_3(OH)_9(H_2O)$ ) from the Jenolan Caves, Australia. *Spectrochim. Acta Mol. Biomol. Spectrosc.* 83 (1), 106–111. <https://doi.org/10.1016/j.saa.2011.07.088>. ISSN 1386-1425.
- Gallant, L.R., Fenton, M.B., Grooms, C., Bogdanowicz, W., Stewart, R.S., Clare, E.L., et al., 2021. A 4,300-year history of dietary changes in a bat roost determined from a tropical guano deposit. *J. Geophys. Res.: Biogeosciences* 126, e2020JG006026. <https://doi.org/10.1029/2020JG006026>.
- Galli, C., Rossi, M., Santi, G., 2005. *URSUS spelaeus Rosenmüller, 1794* from the VENETIAN Region of northern Italy: preliminary notes on its evolutionary path. *Geol. Alpine* 2, 107–113.
- Ghezzo, E., Berté, D.F., Sala, B., 2014. The revaluation of galician canidae, felidae and mustelidae of the cerè cave (verona, northeastern Italy). *Quat. Int.* 339–340, 76–89. <https://doi.org/10.1016/j.quaint.2012.12.031>.
- Goldberg, P., Macphail, R.I., Carey, C., Zhuang, Y., 2022. Practical and Theoretical Geoarchaeology. John Wiley & Sons.
- Gonzato, G., Chignola, R., Rossi, G., 2017. Basalt Intrusions in Palaeokarst Caves in the Central Lessini Mountains (Venetian Prealps, Italy) ACTA CARSOLOGICA 46/1. POSTOJNA, pp. 33–45.
- Greguss, P., 1955. Xilotomische Bestimmung der heute lebeden Gymnospermen. Akadémiai Kiadó, Budapest.
- Haller, S., 2022. Guano extraction in atlantic patagonia (1840–1880). *Int. J. Marit. Hist.* 34 (2), 282–303. <https://doi.org/10.1177/08438714221097017>, 2022.
- IUSS Working Group WRB, 2015. World Reference Base for Soil Resources 2014, update 2015 International soil classification system for naming soils and creating legends for soil maps. In: *World Soil Resources Reports*, vol 106. FAO, Rome, p. 192.
- Ivy-Ochs, S., Kerschner, H., Maisch, M., Christl, M., Kubik, P.W., Schlüchter, C., 2009. Latest pleistocene and holocene glacier variations in the European Alps. *Quat. Sci. Rev.* 28, 2137–2149. <https://doi.org/10.1016/j.quascirev.2009.03.009>.
- Joannin, S., Vanniere, B., Galop, D., Peyron, O., Haas, J.N., Gilli, A., Chapron, E., Wirth, S.B., Anselmetti, F., Desmet, M., Magny, M., 2013. Climate and vegetation changes during the Altglacial and early-middle holocene at lake lendro (southern Alps, Italy). *Clim. Past* 9, 913–933. <https://doi.org/10.5194/cp-9-913-2013>.
- Johnson, J., Vincent, M., 2020. Tracing heavy metals in urban ecosystems through the study of bat guano - a preliminary study from Kerala, India. *J. Threat. Taxa* 12 (10), 16377–16379. <https://doi.org/10.11609/jott.6225.12.10.16377-16379>.
- Larocque, I., Finsinger, W., 2008. Late-glacial chironomid-based temperature reconstructions for Lago Piccolo di Avigliana in the southwestern Alps (Italy). *Palaeogeogr. Palaeoclimatol. Palaeoecol.* 257, 207–223.
- Manzella, G., Fontana, A., Marín-Arroyo, A.B., Agudo Pérez, L., Peresani, M., Duches, R., 2024. Palaeoecology of alpine mid-mountain (trentino, Italy) between Greenland interstadial 1 and early holocene. Carbon and nitrogen isotope analysis of ibex and red deer. *Quat. Sci. Rev.* 328, 108549. <https://doi.org/10.1016/j.quascirev.2024.108549>.
- Margaritora, D., Dozio, A., Chelidonio, G., Turrini, M.C., Peresani, M., 2020. The lower and middle palaeolithic settlements in the baldo-lessini mountains. Results from a gis investigation. *Alpine and Mediterranean Quaternary* 33 (1), 115–132. <https://doi.org/10.26382/AMQ.2020.13>.
- Medina-Alcaide, M.Á., Vandevalde, S., Quiles, A., et al., 2023. 35,000 years of recurrent visits inside Nerja cave (Andalusia, Spain) based on charcoals and soot micro-layers analyses. *Sci. Rep.* 13, 5901. <https://doi.org/10.1038/s41598-023-32544-1>.
- Miko, S., Kuhta, M., Kapelj, S., 2001. Bat guano influence on the geochemistry of cave sediments from modrić cave, Croatia. *Int. Congr. Speleol.* <https://doi.org/10.13140/2.1.4853.2483>.
- Miko, S., Kuhta, M., Kapelj, S., 2002. Environmental baseline geochemistry of sediments and percolating waters in the Modrić, Cave Croatia. *Acta Carsologica* 5, 5. <https://doi.org/10.3986/ac.v3i11.409>.
- Misra, P.K., Gautam, N.K., Elangovan, V., 2019. Bat guano: a rich source of macro and microelements essential for plant growth. *Annals of Plant and Soil Research* 21 (1), 82–86.
- Moldovan, O.T., Mihevc, A., Miko, L., Constantin, S., Meleg, I., Petculessu, A., Bosák, P., 2011. Invertebrate fossils from cave sediments: a new proxy for pre-Quaternary paleoenvironments. *Biogeosciences* 8, 1825–1837. <https://doi.org/10.5194/bg-8-1825-2011>.
- Moldovan, O.T., Kovac, L., Stuart, H., 2018. Cave Ecology. <https://doi.org/10.1007/978-3-319-98852-8>.
- Montoya, C., Duches, R., Fontana, F., Peresani, M., Visentin, D., 2018. In: Averbouh, A., Bonnet-Jacquemet, P., Cleyet-Merle, J.-J.dirs (Eds.), Peuplement tardiglaciaire et holocène ancien des Préalpes de la Vénétie (Italie Nord Orientale): éléments de confrontation, pp. 193–202. L’Aquitaine à la fin des temps glaciaires. Les sociétés de la transition du Paléolithique final au début du Mésolithique dans l’espace Nord aquitain. PALEO, numéro spécial.
- Mulec, J., Dietersdorfer, E., Üstüntürk-Onan, M., Walochnik, J., 2016. Acanthamoeba and other free-living amoebae in bat guano, an extreme habitat. *Parasitol. Res.* 115 (4), 1375–1383. <https://doi.org/10.1007/s00436-015-4871-7>. *Epub* 2015 Dec 17. PMID: 26678653.
- Munsell Soil Color Charts, 2000. Munsell Soil Color Charts e Revised Edition. New Windsor.
- Murphy, C.P., 1986. Thin Section Preparation of Soils and Sediments. AB Academic Publishers, Berkhamsted, p. 149.

- Mussi, M., Peresani, M., 2011. Human settlement of Italy during the younger Dryas. *Quat. Int.* 242, 360–370.
- Nannini, N., Duches, R., Fontana, A., Romandini, M., Boschin, F., Crezzini, J., Peresani, M., 2022. Marmot hunting during the Upper Palaeolithic: the specialized exploitation at Grotte di Pradis (Italian pre-Alps). *Quat. Sci. Rev.* 277, 107364. <https://doi.org/10.1016/j.quascirev.2021.107364>.
- Naudinot, N.A., Tomasso, A., Tozzi, C., Peresani, M., 2014. Changes in mobility patterns as a factor of  $^{14}\text{C}$  date density variation in the Late Epigravettian of Northern Italy and Southeastern France. *J. Archaeol. Sci.* 52, 578–590. <https://doi.org/10.1016/j.jas.2014.05.021>.
- Nicosia, C., Stoops, G. (Eds.), 2017. Archaeological Soil and Sediment Micromorphology. <https://doi.org/10.1002/978111941065>.
- North Greenland Ice Core Project Members, 2007. 50 year means of oxygen isotope data from ice core NGRIP. PANGAEA. <https://doi.org/10.1594/PANGAEA.586886>.
- Onac, B.P., 2012. Minerals. In: Culver, D.C., White, W.B. (Eds.), Encyclopedia of Caves, second ed. Elsevier, New York, pp. 499–508. <https://doi.org/10.1016/B978-0-12-383832-2.00072-4>.
- Pasquetti, F., Zanchetta, Giovanni, Caron, Benoit, Noel, Julie, Avanzinelli, Riccardo, Vannière, Boris, Desmet, Marc, Magny, Michel, Wagner, Bernd, Dallai, Luisa, Fulignati, Paolo, Bini, Monica, Banesch, Ilaria, 2025. Lead legacy of pre-industrial activities in lake sediments: the case study of the Lake Accesa (Southern Tuscany, Italy). *Anthropocene* 49, 100464. <https://doi.org/10.1016/j.ancene.2025.100464>. ISSN 2213-3054.
- Pedrotti, A., Salzani, P., Cavulli, F., Carotta, M., Angelucci, D., Salzani, L., 2015. L'insediamento di Lugo di Grezzana (Verona) nel quadro del primo Neolitico padano alpino. In: Atti della XLVII riunione scientifica dell'Istituto Italiano di Preistoria e Protostoria, pp. 95–107. Padova 5–9 novembre 2013, Firenze.
- Peresani, M., 2009. Osservazioni sul modo di vita dei Neanderthaliani durante lo stadio isotopico 3 nelle Alpi italiane. "Gortania", Atti del Museo di Storia Naturale del Friuli 31, 87–96. Udine.
- Peresani, M., Cremaschi, M., Ferraro, F., Falguères, C., Bahain, J.J., Gruppioni, G., et al., 2008. Age of the final middle palaeolithic and uluzzian levels at Fumane cave, northern Italy, using  $^{14}\text{C}$ , ESR,  $^{234}\text{U}/^{230}\text{Th}$  and thermoluminescence methods. *J. Archaeol. Sci.* 35 (11), 2986–2996.
- Peresani, M., Monegato, G., Ravazzi, C., Bertola, S., Margaritora, D., Breda, M., Fontana, A., Fontana, F., Janković, I., Karavanic, I., Komšo, D., Mozzì, P., Pini, R., Furlanetto, G., Giovanni, Maria De Amicis M., Perhoč, Z., Posth, C., Ronchi, L., Rossato, S., Vukosavljević, N., Zerboni, A., 2021. Hunter-gatherers across the Great adriatic-Po region during the last glacial maximum: environmental and cultural dynamics. *Quat. Int.* 581–582, 128–163. <https://doi.org/10.1016/j.quaint.2020.10.007>.
- Pignatti, S., 1982. Flora d'Italia. I-II-III. Edagricole, Bologna.
- Pini, R., Ravazzi, C., Donegana, M., 2009. Pollen stratigraphy, vegetation and climate history of the last 215ka in the Azzano Decimo core (plain of Friuli, north-eastern Italy). *Quat. Sci. Rev.* 28, 1268–1290.
- Pini, R., Ravazzi, C., Reimer, P.J., 2010. The vegetation and climate history of the last glacial cycle in a new pollen record from Lake Fimon (southern Alpine foreland, N-Italy). *Quat. Sci. Rev.* 29, 3115–3137.
- Queffelec, A., Bertran, Pascal, Bos, Teddy, Lemée, Laurent, 2018. Mineralogical and organic study of bat and chough guano: implications for guano identification in ancient contexts. *J. Cave Karst Stud.* 80 (2), 49–65. <https://doi.org/10.4311/2017es0102>.
- Rasmussen, S.O., Bigler, M., Blockley, S.P., Blunier, T., Buchardt, S.L., Clausen, H.B., Cvijanovic, I., Dahl-Jensen, D., Johnsen, S.J., Fischer, H., Gkinis, V., Guillemin, M., Hoek, W.Z., Lowe, J.J., Pedro, J.P., Popp, T., Seierstad, I.K., Steffensen, J.P., Svensson, A.M., Vallelonga, P., Vinther, B.M., Walker, M.J., Wheatley, J.J., Winstrup, M., 2014. A stratigraphic framework for abrupt climatic changes during the Last Glacial period based on three synchronized Greenland ice-core records: refining and extending the INTIMATE event stratigraphy. *Quat. Sci. Rev.* 106, 14e28. <https://doi.org/10.1016/j.quascirev.2014.09.007> 0070277e3791 g and extending the INTIMATE event stratigraphy. *Quaternary science reviews*, 106, 14–28.
- Ravazzi, C., Peresani, M., Pini, R., Vescovi, E., 2007. The Late Glacial in the Italian Alps and in the Po Plain: stratigraphy, vegetation history and human peopling. *Il Quaternario Italiano J. Quaternary Sci.* 20 (2), 163.
- Reeves, A.D., Patton, D., 2005. Feaecal Sterols as indicators of sewage contamination in estuarine sediments of the Tay Estuary, Scotland: an extended baseline survey. *Hydrol. Earth Syst. Sci.* 9, 81–94, 2005. [www.copernicus.org/EGU/hess/hess/9/81/](http://www.copernicus.org/EGU/hess/hess/9/81/).
- Reid, R.E.B., Waples, J.T., Jensen, D.A., Edwards, C.E., Liu, X., 2022. Climate and vegetation and their impact on stable C and N isotope ratios in bat guano. *Front. Ecol. Evol.* 10, 929220. <https://doi.org/10.3389/fevo.2022.929220>.
- Reimer, P.J., Austin, W.E.N., Bard, E., Bayliss, A., Blackwell, P.G., Ramsey, C.B., Butzin, M., Cheng, H., Edwards, R.L., Friedrich, M., et al., 2020. The IntCal20 Northern Hemisphere radiocarbon age calibration curve (0–55 cal kBP). *Radiocarbon* 62 (4), 725–757. <https://doi.org/10.1017/RDC.2020.41>.
- Riordan, K.J., Field, J.S., Dudgeon, J.V., 2021. Investigating geoarchaeological deposits from nailhehe cave in the sigatoka river valley viti levu, Fiji. *J. Archaeol. Sci.: Report* 40, 103202.
- Romandini, M., Peresani, M., Gurioli, F., Sala, B., 2012. Marmota marmota, the most predated species at Grotta del Clusantin. Insights from an unusual case-study in the Italian Alps. *Quat. Int.* 252, 184–194. <https://doi.org/10.1016/j.quaint.2011.03.016>.
- Ruiz-Redondo, A., Vukosavljević, N., Tomasso, A., Peresani, M., Davies, W., Vander, Linden M., 2022. Mid and Late Upper Palaeolithic in the Adriatic Basin: chronology, transitions and human adaptations to a changing landscape. *Quat. Sci. Rev.* 276, 107319. <https://doi.org/10.1016/j.quascirev.2021.107319>.
- Salzani, L., 1987. Sant'Anna d'Alfaedo, Ponte di Veja. *Quaderni di Archeologia del Veneto III*, 108–109.
- Schmidt, I., Gehlen, B., Winkler, K., Arrizabalaga, A., Arts, N., Bicho, N., Crombé, Ph., Eriksen, B.V., Grimm, S.B., Kapustka, K., Langlais, M., Mevel, L., Naudinot, N., Nerudová, Z., Niekuš, M., Peresani, M., Riede, F., Sauer, F., Schön, W., Sobkowiak-Tabaka, I., Vandendriessche, H., Weber, M.J., Zander, A., Zimmermann, A., Maier, A., 2025. Large scale and regional demographic responses to climatic changes in Europe during the Final Palaeolithic. *PLoS One* 20 (4), e0310942. <https://doi.org/10.1371/journal.pone.0310942>.
- Schweingruber, F.H., 1990. Anatomy of European Woods. Haupt, Stuttgart.
- Sokol, E.V., Kozlikin, M.B., Kokh, S.N., Nekipelova, A.V., Kulik, N.A., Danilovsky, V.A., et al., 2022. Phosphate record in Pleistocene-holocene sediments from Denisova cave: formation mechanism and archaeological implications. *Minerals* 12, 555. <https://doi.org/10.3390/min12050553>.
- Stephens, M., Rose, J., Gilbertson, D.D., 2017. Post-depositional alteration of humid tropical cave sediments: micromorphological research in the Great cave of niah, sarawak, borneo. *J. Archaeol. Sci.* 77, 109–124.
- Stoops, G., 2021. Guidelines for Analysis and Description of Soil and Regolith Thin Sections. ASA, CSSA, SSSA Books and Wiley & Sons, Inc.
- Stoops, G., Marcelino, V., Mees, F. (Eds.), 2018. Interpretation of Micromorphological Features of Soils and Regoliths, second ed. Elsevier, Amsterdam, p. 1000.
- Supplement to: North Greenland Ice Core Project Members, 2004. High-resolution record of Northern Hemisphere climate extending into the last interglacial period. *Nature* 431, 147–151. <https://doi.org/10.1038/nature02805>.
- Tagliacozzo, A., Cassoli, P.F., 1994. La macrofaune de l'Abri Soman (Val d'Adige-Italie). *Preistoria Alp.* 28, 181–192.
- Tagliacozzo, A., Fiore, I., 2009. Hunting strategies in a mountain environment during the Late Glacial in northeastern Italy. *Preist. Alp.* 44, 79–93.
- Torok, A.I., Casoni, D., Senila, M., Tanaselia, C., Covaci, E., Hoaghia, M.-A., Neag, E., Cedar, O., Levei, E.A., Arghir, R., Moldovan, O.T., Constantin, S., Frentiu, T., 2024. Spatial variability and hydro/geochemical profiling of the elemental composition of mineral deposits and drip water from caves using unsupervised chemometric modelling. *Chem. Geol.* 646, 121903. <https://doi.org/10.1016/j.chemgeo.2023.121903>. ISSN 0009-2541.
- Tsalikis, A., Waters, M.N., Campbell, J.W., 2021. Methods and analysis of bat guano cores from caves for paleoecology. *J. Cave Karst Stud.* 84, 141–150.
- Vernet, J.-L., Ogereau, P., Figueiral, I., Machado Yanes, C., Uzquiano Oller, P., 2001. Guide d'identification des charbons de bois pré historiques et récents: Sud-Ouest de l'Europe, France. enisule ib erique et îles Canaries. CNRS Editions, Paris.
- Vernier, E., 2000. Interessanti ricatture di Chiroterri Vespertilionidi in grotte della regione Veneto. In: Atti della I Conferenza interregionale sull'Ecologia e Distribuzione dei Chiroterri Italiani, pp. 166–170. Vicenza, 2000.
- Vescovi, E., Ravazzi, C., Arpenti, E., Finsinger, W., Pini, R., Valsecchi, V., Wick, L., Ammann, B., Tinner, W., 2007. Interactions between climate and vegetation during the Lateglacial period as recorded by lake and mire sediment archives in Northern Italy and Southern Switzerland. *Quat. Sci. Rev.* 26 (11–12), 1650–1669. <https://doi.org/10.1016/j.quascirev.2007.03.005>.
- Villagrán, X.S., Huisman, D.J., Mentzer, S.M., Miller, C.E., Jans, M.M., 2017. Bone and other Skeletal tissues. In: Nicosia, C., Stoops, G. (Eds.), Archaeological Soil and Sediment Micromorphology. John Wiley & Sons, Ltd, Chichester, pp. 11–33.
- White, W.B., 2007. Cave sediments and paleoclimate. *J. Cave Karst Stud.* 69, 76–93. [https://digitalcommons.usf.edu/kip\\_articles/784](https://digitalcommons.usf.edu/kip_articles/784).
- Williams, A.J., Pagliai, M., Stoops, G., 2018. Physical and biological surface crusts and seals. In: Interpretation of Micromorphological Features of Soils and Regoliths. Elsevier, pp. 539–574.
- Wurster, C.M., Munksgaard, N., Zwart, C., Bird, M., 2015. The biogeochemistry of insectivorous cave guano: a case of study from insular Southeast Asia. *Biogeochem* 124, 163–175. <https://doi.org/10.1007/s10533-015-0089-0>.